Design of a Portable and Affordable Biosensor Platform Device

By

Songtian Bai

A thesis submitted in partial fulfillment of the requirements for the degree of

Master of Science

in

Biomedical Engineering

Department of Electrical and Computer Engineering

University of Alberta

Abstract

Metabolomics is a rapidly growing field that focuses on identifying and measuring the collection of chemicals present within a biological system. These chemicals, known as metabolites, play a crucial role in the functioning of the body and can provide valuable insights into various physiological processes. As a result, metabolomics studies have been utilized in a wide range of health monitoring applications, including screening for early-stage cancer. Traditionally, high-end analytical chemistry tools such as a spectrophotometer have been used to measure metabolites in biological samples through the application of colorimetry. These instruments, however, are typically expensive and require skilled technicians to operate. Due to these limitations, they are usually found in centralized labs and are not suitable for in-clinic or bedside use. Teaming up with researchers across the world, the research group I am a part of is attempting to address the issue of colorectal cancer screening in developing countries. Finally, we exceeded the requirements and developed a low-cost, hand-held, point-of-care optical sensor platform for general colorimetric-based metabolomic testing applications. This platform is equipped with a 3D printed light-tight case that contains light-emitting diodes (LED), sensors, microcontrollers, and a Bluetooth chip for wireless communications to an Android tablet. The performance of this sensor is evaluated using a colorimetric creatinine assay. Creatinine, a metabolite used to normalize urinary metabolite concentrations, was assayed using the Jaffe reaction, a commonly used method in laboratory settings. First, the color sensors were evaluated for stability using yellow-colored water that mimicked the Jaffe reaction color product. Next, the sensor was tested for accuracy using the Jaffe creatinine-picrate complex, which produced yellow-orange

colored products. The sensor was able to detect creatinine concentrations ranging from 3.80 mM to 50.28 mM, which is well within the physiological range expected in human urine. When compared to a spectrophotometer, which is considered the gold standard for this type of analysis, the sensor was found to be highly accurate. The sensor was able to accurately measure creatinine standards and high, medium, and low concentrations of spiked urine samples. One of the major advantages of this sensor is its cost-effectiveness and ease of use. Additionally, the sensor can be expanded to measure other metabolites via colorimetric assays, further increasing its versatility and utility in a wide range of applications. Furthermore, this thesis will address the developed workstation device on which the sensor can be mounted, and this device will serve as an assistant in the metabolite assay process by automating major steps that could be time-consuming or experience-dependent. Overall, this low-cost, hand-held, point-of-care optical sensor platform has the potential to revolutionize the field of metabolomics by providing a simple, cost-effective, and reliable method for measuring metabolites in biological samples. This can greatly benefit the medical field by providing a more accessible and efficient way of performing diagnostic tests, ultimately improving patient outcomes.

Preface

This thesis is an original work by Songtian Bai. Some of the research conducted for this thesis forms part of an international research collaboration, led by Professor P. Kingham at the Sloan Kettering Institute for Cancer Research, with Professor D. Wishart being the lead collaborator at the University of Alberta. The sensor device and workstation referred to in chapter 3 and 5 were designed with the help of all members of the Tricca Inc. team. The data collection and concluding analysis in chapter 4 contains my original works as well as help from Wishart lab chemistry team members to set up experiments.

Some of the material presented in this thesis has been included in the following publications:

[1] S. Bai, J. Cook, S. MacKay, P. Gonzalez-Vasquez, D. Wishart, J. Chen, and G. Davies. "Design of an adaptable sensing platform for metabolomic sensing," in Proceedings of the 8th International Electronic Conference on Sensors and Applications, 1–15 November 2021, MDPI: Basel, Switzerland, doi:10.3390/ecsa-8-11339

[2] S. Bai, P. Gonzalez-Vasquez, C. Torres-Calzada, S. MacKay, J. Cook, Y. Khaniani, G. Davies, P. Kovur, J. Chen, and D. S. Wishart. "Development of a Point-of-Care Color Sensitive Metabolomic Sensor Platform," [Unpublished manuscript].

Acknowledgments

Table of Contents

List of Tables

List of Figures

Chapter 1

Introduction

The University of Alberta laboratory I am a part of (Tricca Technology Inc.) launched a project together with Memorial Sloan Kettering Cancer Center, Obafemi Awolowo University, and Metabolomic Technologies Inc. that aims to make a point-of-care (POC) metabolomics urine test to diagnose patients with colorectal cancer(CRC). Colorectal cancer is a growing problem in low- and middle-income countries, and screening methods with high sensitivity are limited due to their cost and accessibility. With the help of the Wishart lab chemistry team, the colorimetric assays are being developed based on the data that is collected from Nigeria. Combined with the developed sensor device, the proposed test will allow for affordable POC colorectal cancer screening and diagnosis of earlier-stage patients. The result of testing will show a level of accuracy comparable with the traditional spectrophotometers while unaffected by environmental factors.

1.1 Spectroscopy Background

Spectroscopy, which is the study of the absorption and emission of light by matter, plays a crucial role in various scientific disciplines[1]. One of the fundamental principles to understand when investigating the interaction of light with a sample is the Beer-Lambert Law[2], which is a combination of Beer's Law and Lambert's Law.

Beer's Law, formulated by August Beer in the mid-19th century, describes the relationship between the absorption of light by a solution and the concentration of the absorbing species within that solution[3]. According to Beer's Law, the absorbance of a solution is directly proportional to the concentration of the absorbing substance:

$$A = \varepsilon cl \qquad (1.1)$$

Here, ε represents the molar absorption coefficient or molar absorptivity, a constant specific to the absorbing substance and the wavelength of light used. The molar absorption coefficient indicates how strongly a substance absorbs light at a particular wavelength. The concentration (c) is the amount of the absorbing substance present in the solution, typically expressed in moles per liter (mol/L). Finally, l signifies the optical path length, the distance that light travels through the solution, typically measured in centimeters (cm).

Lambert's Law, formulated by Johann Heinrich Lambert, complements Beer's Law. Lambert's Law states that the absorbance of a solution is directly proportional to the path length of light through the solution:

$$A = k * l \qquad (1.2)$$

In this equation, k is a proportionality constant.

The Beer-Lambert Law combines Beer's Law and Lambert's Law, providing a more comprehensive relationship that accounts for both concentration and path length:

$$A = \varepsilon cl \qquad (1.1)$$

The Beer-Lambert Law states that the absorbance of a solution is directly proportional to the product of the molar absorption coefficient, concentration, and path length[4]. It provides a linear relationship between absorbance and these three factors,

allowing for quantitative measurements of the concentration of absorbing species within a solution.

Colorimetry is a technique within spectroscopy that focuses on the measurement of light in the visible spectrum. It involves the visual perception of color and relates the color of a sample to a specific concentration or property of interest[5]. Colorimetry is used to determine the concentration of colored compounds in solutions by the application of the principles of Beer's Law and the Beer-Lambert Law. By applying these principles to colored solutions with similar properties, the concentration of any colored compounds contained within a solution can be determined. This technique provides valuable information in various fields such as biochemistry[6], environmental analysis[7], and clinical diagnostics[8][9].

In colorimetry, the measurement of color is often performed using a spectrophotometer[10], which is a standard piece of equipment used in many spectroscopy studies. A spectrophotometer combines a spectrometer, which outputs light at controlled wavelengths[11], and a photometer, which detects and measures the electromagnetic radiation of received light[12], into a single device, enabling the measurement of the absorbance of light at specific wavelengths by a sample solution[13].

The spectrophotometer works by first generating monochromatic light, which refers to light consisting of a single wavelength, at controlled wavelengths using a spectrometer. This can be achieved by passing light through either a prism or a diffraction grating, causing the light to disperse into its component wavelengths[14]. Subsequently, the dispersed light is directed onto the sample solution, allowing the interaction of various wavelengths of light with the colored compounds present in the solution.

As per Beer's Law and the Beer-Lambert Law, the absorption of light by the sample is directly proportional to the concentration of the colored compounds. The spectrophotometer's photometer component detects and measures the electromagnetic radiation of the received light after it passes through the sample solution. This measurement allows for the quantification of the absorbance, which can then be correlated with the concentration of the colored compounds using the principles of Beer's Law.

By utilizing a spectrophotometer, the colorimetric analysis of a sample can be performed accurately and precisely. The instrument's ability to control the wavelengths of light and detect the resulting absorbance enables quantitative measurements of the concentration of colored compounds in a solution.

The generation of monochromatic light from the incident light source prior to interacting with the sample constitutes a significant cost factor in a spectrophotometer[15]. True monochromatic lighting solutions do not exist, they are simply made up of a very narrow band of light in the spectrum[16].

However, let us consider using a wide-band polychromatic lighting[17] solution in cases where the signal molecule has either high molar absorptivity or the concentration of the molecule in the solution is relatively high. The work of this thesis will demonstrate the effect on the measured absorption value from the photometer when using a polychromatic incident light source paired with a highly concentrated sample, and how the measured absorbance will be quantified.

In summary, colorimetry is a spectroscopy technique that utilizes the principles of Beer's Law and the Beer-Lambert Law to establish a relationship between the color of a sample and its concentration or specific property. The measurement of color through

colorimetry is commonly performed using a spectrophotometer, which enables accurate and precise analysis by controlling the wavelengths of the incident light and measuring the resulting absorbance. The integration of colorimetry and spectrophotometry provides a powerful approach for quantitative analysis in various fields, including biochemistry, environmental science, and clinical diagnostics.

1.2 Metabolomics Background

Metabolomics is an emerging field of study that aims to comprehensively analyze and understand the metabolome, which refers to the complete set of small molecules or metabolites present within a biological system[18]. These metabolites are products of various cellular processes influenced by genetic, environmental, and physiological factors[19][20]. By characterizing the metabolome, metabolomics provides valuable insights into the biochemical pathways and physiological status of an organism.

The potential applications of metabolomics have gained significant attention across a wide range of areas, including nutrition[21], disease diagnosis[22], and personalized medicine[23]. A notable application lies in the assessment of dietary intake[24]. Metabolomic profiling enables the detection and quantification of specific metabolites in biofluids or tissues that are indicative of dietary components or patterns. By analyzing the metabolites present, researchers can gain insights into an individual's dietary habits, nutrient intake, and the impact of diet on health[25].

Another important application of metabolomics lies in the prediction and diagnosis of diseases, such as heart disease[26] and cancer[27]. Metabolomic profiling can identify unique patterns or signatures of metabolites associated with specific diseases. In the case of heart disease, metabolomics has been used to identify metabolites that are

linked to the risk of developing cardiovascular conditions[28]. By analyzing the metabolome, researchers can potentially identify individuals at a higher risk of heart disease and develop targeted interventions for prevention and treatment.

In the realm of cancer, metabolomics has shown promising potential in improving early detection[29], prognosis[30], and treatment response assessment[31]. Different types of cancer exhibit distinct metabolic alterations, which can be captured through metabolomic profiling[32]. Metabolites can serve as biomarkers, which are measurable indicators that provide information about the presence, severity, or prognosis of a disease. In cancer research, biomarkers play a critical role in early detection, personalized treatment selection, and monitoring treatment response[33].

A biomarker panel refers to a combination of multiple biomarkers that collectively provide a more accurate and comprehensive assessment of diseases[34]. In the context of cancer, a biomarker panel may consist of multiple metabolites that exhibit consistent alterations in cancer samples. The analysis of such panels allows for improved diagnostic accuracy and predictive capabilities, as the combination of multiple biomarkers provides a more holistic view of the underlying biological processes associated with the disease.

Metabolomic analysis in cancer research involves the use of advanced techniques such as mass spectrometry (MS), nuclear magnetic resonance spectroscopy (NMR), and liquid chromatography (LC) coupled with mass spectrometry[35][36]. These techniques enable the identification and quantification of metabolites present in biological samples, allowing for comprehensive metabolomic profiling. Through the application of these methods, specific metabolites or panels of metabolites that exhibit significant associations with particular types or stages of cancer can be identified.

In summary, metabolomics is a rapidly expanding field that aims to characterize the metabolome and understand the intricate interrelationship between metabolites, genetic factors, environmental influences, and physiological processes. It encompasses diverse applications in areas such as nutrition, disease diagnosis, and personalized medicine. Metabolomics holds promise for early detection, prognosis, and treatment optimization of cancer. By identifying specific metabolite alterations and utilizing biomarker panels, researchers can learn about the complex metabolic alterations associated with cancer and develop innovative strategies for diagnosis and therapeutic interventions.

1.3 Electrochemical and colorimetric reactions

Electrochemical reactions encompass the transfer of electrons between species and typically take place at the interface of an electrode and an electrolyte solution[37]. These reactions involve oxidation and reduction processes, wherein one species loses electrons (oxidation) while another species gains electrons (reduction). Electrochemical reactions can be used to study various phenomena, including the determination of oxidation states[38], the measurement of redox potentials[39], and the investigation of reaction kinetics[40]. They are widely employed in fields such as electrochemistry, energy storage and conversion, corrosion studies, and sensing technologies[41]. By harnessing electron transfer events, electrochemical reactions provide valuable insights into the behavior of molecules and materials in diverse chemical and biological systems.

While electrochemical reactions offer advantages in various fields, they are not commonly used as the primary method in metabolomics studies for several reasons. Firstly, metabolomics aims to analyze a wide range of metabolites, making it challenging

for electrochemical reactions to provide the necessary selectivity and sensitivity across the entire metabolome. Additionally, complex biological samples encountered in metabolomics, such as urine or blood, contain various interfering substances that can affect the accuracy of electrochemical analysis[42]. Furthermore, the wide dynamic range of metabolite concentrations in metabolomics requires methods capable of accurately quantifying compounds at both high and low abundance, which may pose limitations for electrochemical techniques[43]. Moreover, the validation and standardization of electrochemical methods in metabolomics are not as advanced as other established techniques like mass spectrometry or nuclear magnetic resonance spectroscopy. While electrochemical reactions can be useful for targeted analysis of specific redox-active metabolites within metabolomics, they are not commonly employed as the primary approach for comprehensive metabolite profiling.

Colorimetric reactions are widely employed in metabolomics due to their simplicity, cost-effectiveness, and broad applicability[44]. In metabolomics, colorimetric assays offer a convenient and rapid means to detect and quantify a broad range of analytes in biological samples. These assays involve specific interactions between metabolites and reagents, resulting in color changes that can be easily measured visually or spectrophotometrically. The versatility of colorimetric reactions enables the detection of various metabolite classes, and their scalability makes them suitable for high-throughput analysis[45]. Furthermore, colorimetric assays are cost-effective, as they require simple equipment and readily available reagents. By correlating the intensity of color changes with metabolite concentrations, quantitative measurements can be obtained, facilitating comparative analyses. Overall, the use of colorimetric reactions in metabolomics provides

a practical and affordable approach to metabolite analysis, making them valuable tools in research and clinical applications.

An example of colorimetry application is the Jaffe reaction which is a widely used non-enzymatic method for determining the concentration of creatinine in blood or urine samples[46]. Creatinine, a metabolite produced by muscle metabolism, serves as an important indicator of kidney function. The Jaffe reaction involves the interaction of creatinine and picric acid, resulting in the formation of a colored complex. The intensity of the color change is directly proportional to the concentration of creatinine in the sample [47]. By measuring the absorbance of the colored complex using a spectrophotometer, the concentration of creatinine can be quantified, providing valuable information about kidney health and overall metabolism.

1.4 Point-Of-Care testing

In metabolomics studies, the data collection process often requires time-sensitive approaches to capture dynamic changes in metabolite levels. Point-of-care (POC) testing is a valuable approach employed to address this need. POC testing involves performing diagnostic tests near the patient, outside of a traditional laboratory setting. It enables rapid and on-site analysis of biological samples, eliminating the need for sample transportation and extensive laboratory infrastructure[48].

Overall, POC testing offers the opportunity for real-time analysis of metabolites in various biological samples, including blood, urine, or saliva. Portable and user-friendly devices, such as handheld analyzers or biosensors[49], are utilized for POC testing. These devices are designed to detect and quantify specific metabolites of interest within minutes, providing immediate results.

In metabolomics, POC testing offers several advantages. Firstly, it enables timely decision-making by allowing researchers and clinicians to monitor metabolic changes in response to interventions or during specific time windows. Additionally, it alleviates the logistical challenges associated with sample collection, transport, and centralized laboratory analysis, making it particularly suitable for fieldwork, remote areas, or resource-limited settings[50]. Furthermore, it can be integrated with automated data analysis and interpretation algorithms, streamlining the metabolomic workflow and enhancing data processing efficiency[51]. This integration enables real-time data interpretation, facilitating rapid insights into metabolite patterns and their association with specific conditions or diseases.

Overall, POC testing in metabolomics plays a vital role in enabling time-sensitive data collection, enhancing the efficiency of metabolomic studies, and facilitating point-of-care diagnostics. It offers the potential for immediate results, on-site analysis, and real-time monitoring of metabolite dynamics, contributing to advancements in personalized medicine, disease management, and understanding of metabolic processes.

Colorimetry using a spectrophotometer is a commonly used method in metabolomics for measuring metabolite concentrations in biological samples. However, in the context of POC testing, it is necessary to obtain results on-site, especially in fieldwork settings where access to laboratory equipment is limited[52].

While spectrophotometers are highly accurate and precise, they are expensive, often costing more than $4,000 US dollars. Moreover, they are primarily used in research environments where trained experts operate and analyze the collected data, making them impractical for in-clinic or bedside use. This situation calls for a portable and low-cost

alternative, such as a biosensor, that could be used alongside a developed colorimetric assay while completely replacing the spectrophotometer.

In recent years, miniaturized spectrophotometers that can be used with smartphone ambient light sensors have been developed, allowing for easy data collection and analysis in fieldwork settings where access to a laboratory may not be possible[53][54]. However, these spectrophotometers may not have the same precision and accuracy as traditional spectrophotometers and can be affected by environmental factors.

1.5 Thesis outline

This thesis aims to demonstrate the utilization of quantitative color analysis combined with colorimetric assays for biomarker identification in human urine samples, offering an affordable approach. In the device section, we used a more cost-effective approach to generate a wide spectral bandwidth incident light and conducted additive color analysis on the output light. The metabolite chosen for demonstrating results in this thesis is creatinine, and the assay process involves the preparation of a sample solution with high concentrations of the target molecule, thus reducing the effect of spectrophotometric analysis of complex solutions using wide spectral bandwidth. The programming section will focus on data processing, including the calculation of metabolite concentration using quantitative color analysis. Additionally, the steps taken to automate the project-associated assay processes will also be addressed.

Regarding the cost aspect of the device, specific pricing information will be detailed in the thesis. A thorough analysis of the device's affordability, including the cost of

different manufactured parts will be discussed. This information will help assess the cost-

effectiveness and potential scalability of the device for widespread use in POC settings.

Chapter 2

Sensor design

The project aims to create a portable Point-Of-Care system that any trained personnel can utilize for cancer screening purposes in the field without requiring high-end analytical instruments like a spectrophotometer. The project outlined two goals, one of which was to develop an assay to determine Cancer biomarkers in urine samples. The other goal was to develop a POC device that could be used to measure the biomarkers. We, the team at Tricca, took on the challenge of developing the biosensor device. This chapter will outline the sensor designs and challenges that I have faced during the process.

Three versions of the sensor platform device were developed during my time at the lab: the 96-well plate sensor platform, the 3-well sensor, and the workstation device. The three devices were designed to suit different needs and were to be used in different situations when built. The 96-well plate sensor platform device and the 3-well sensor device are purely sensory-based designs. They can be commanded through Bluetooth to measure a sample, then store the value for sending in future Bluetooth communication. In contrast, the workstation design utilizes the same 3-well sensor device but involves elements of assay automation, which Bluetooth also controls. This chapter will only discuss the elements involved in the 96-well plate sensor platform device and the 3-well sensor; chapter 5 will address the workstation device.

2.1 96-well plate sensor platform design

The 96-well version of the sensor platform design, assembled with help from my fellow research assistants at Tricca, was designed for the purpose of measuring data from the 96-well plates that are often seen in laboratory settings. Most laboratory devices are designed to interface with a standard 96-well plate. For example, multichannel pipettes are spaced out such that each channel can fill one well on a 96-well plate, and the spectrophotometers used by the lab can read samples that are contained within a 96-well plate, the user can even select the specific well they would like to read data from using the accompanying computer program.

My main role at this time was to create an application that would control the device using BLE, then test the app on the alpha model of the device to spot any bugs within the software and at the same time, identify flaws in the physical sensor platform design that either needs urgent fixes or noted for future iterations.
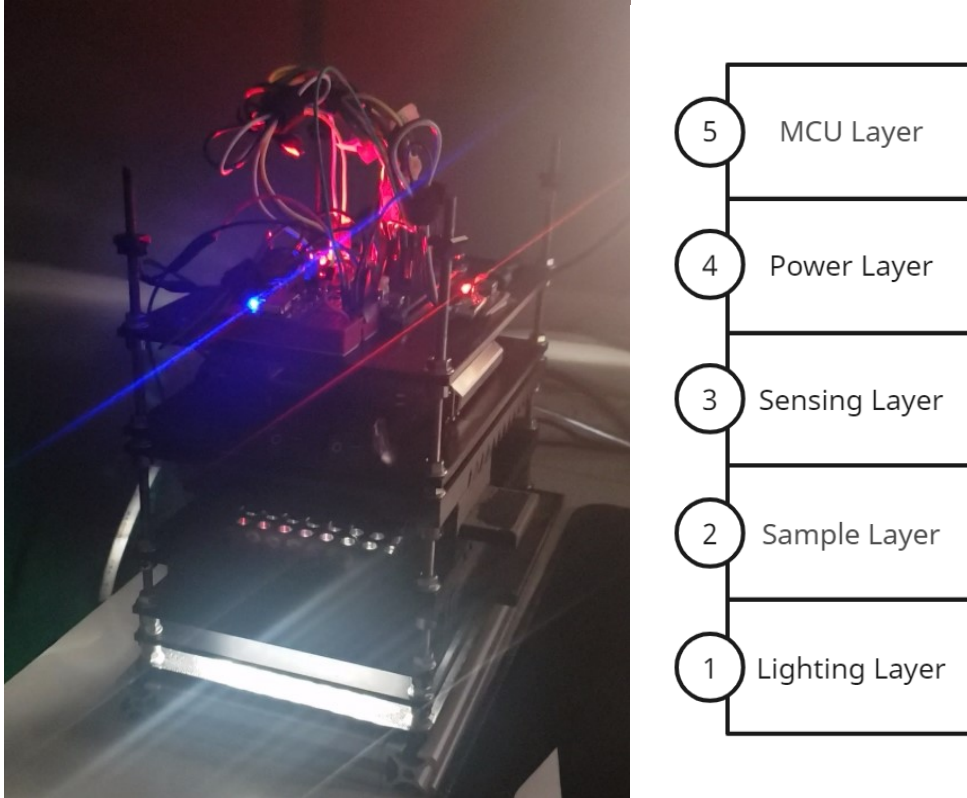
Figure 2.1. 96-well Sensor Device

The device is shown in figure 2.1; the design adopts a sandwich model where each layer would have its own purpose, as shown in ascending order from the bottom. The layers are listed as follows.

The first layer is the lighting layer, and this section contains a Printed Circuit Board(PCB) with 96 white LEDs and a singular multiplexer (MUX), one for each well of the 96-well plate. The LED array is connected such that one column is turned on at one time, and to control which column is turned on, a MUX is used to multiplex the output signals of the microcontroller.

The second layer of the device is the sample layer. It contains the holding tray for the 96-well plate. 96 circular cutouts on the tray line up perfectly with each well in the 96-well plate for unobstructed lighting from the LED directly to the wells.

The third layer is the sensing layer. It contains eight sensor units mounted on a 3D printed sensor mount, orientated into one line, and spaced out so that each sensor will measure one well from a single column on the 96-well plate. The sensor mount can be shifted horizontally to measure all twelve columns of the 96-well plate.

The fourth layer of the device is the power layer. This layer hosts all the power supplies, additional voltage regulators, and power switches. The outlet provides 120V AC which needs to be stepped down to 12V, 5V, and 3.3V such that the LED PCB, Main Controller Unit(MCU) PCB, and sensor modules can be adequately powered.

The fifth and last layer of the device is the MCU layer, which has all the controller PCBs and Bluetooth PCBs mounted on it. Since this layer is the top layer and is fully exposed, we can easily access the components to make modifications.

2.2 Materials list

Item	Supplier	Qty	Cost
Eryone PLA 3d Printing filament	Amazon	1	$ 34.99
M2 screws and nuts pack	McMaster-Carr	1	$ 7.45
M3 screws and nuts pack	McMaster-Carr	1	$ 12.97
PVC silicone wire kit	cbazy	1	$ 24.88
20mm Aluminum T-slotted extrusions	McMaster-Carr	1	$ 6.20
ATMega328P-U	Digi-Key Electronics	1	$ 4.47
16MHz Crystal	Digi-Key Electronics	1	$ 0.46
2 pin phoenix 20 pack	Amazon	1	$ 13.08
6 pin phoenix 10 pack	Amazon	1	$ 10.93
M3 standoff pack	Amazon	1	$ 14.69
male pin header (20)	Digi-Key Electronics	2	$ 6.54
TCA9548APWR Mux	Digi-Key Electronics	1	$ 3.00
TCS34725FNCT-ND	Digi-Key Electronics	8	$ 1.93
MCP73833	Digi-Key Electronics	1	$ 0.91
TPS63021DSJ Buck/Boost	Digi-Key Electronics	1	$ 2.95
PMOS Switch AOD21357	Digi-Key Electronics	1	$ 1.19
Diode SMD26PL-TP	Digi-Key Electronics	1	$ 0.45
Green LED 0805	Digi-Key Electronics	1	$ 0.25
RED LED 0805	Digi-Key Electronics	3	$ 0.27
SPMWH1228FD	Digi-Key Electronics	8	$ 0.22
60 Ohm Resistors (1206)	Digi-Key Electronics	4	$ 0.10
2kOhm Resistor (1206)	Digi-Key Electronics	1	$ 0.10
1kOhm Resistor (1206)	Digi-Key Electronics	1	$ 0.10
10kOhm resistor (1206)	Digi-Key Electronics	24	$ 0.14
150kOhm Resistor (1206)	Digi-Key Electronics	1	$ 0.06
10k NTC Thermistor (1206)	Digi-Key Electronics	1	$ 2.01
JST (S2B-PH-SM4-TB)	Digi-Key Electronics	1	$ 0.53
10uF Capacitor (1206)	Digi-Key Electronics	5	$ 0.27
0.1uF Capacitor (1206)	Digi-Key Electronics	9	$ 0.31

22uF Capacitor (1206)	Digi-Key Electronics	3	$ 0.87
22pF Capacitor (1206)	Digi-Key Electronics	2	$ 0.41
1.5uH Inductor	Digi-Key Electronics	1	$ 1.39
Total:			$ 178.94

Table 2.1. Materials cost and source list

2.3 Three-well sensor platform design

The three-well sensor platform is a redesign of the 96-well sensor platform. The purpose of the design was to cut down on the form factor and make a system that is easier to operate for the end user, especially in the case of the project, where the end user is expected to have minimal specialized knowledge. We have cut down the number of operating sensors within the device from eight to three, but the internal PCB components of this three-well sensor platform can still be adapted to operate on a 96-well plate since there are still eight sensor mounting slots available. This change was made because only three metabolite was required for the purpose of the project, and also, another reason was that the results obtained from the 96-well plates testing showed large discrepancies from sample to sample due to variation in volumes, which affected the optical path length, this was discovered by my peers during their testing.
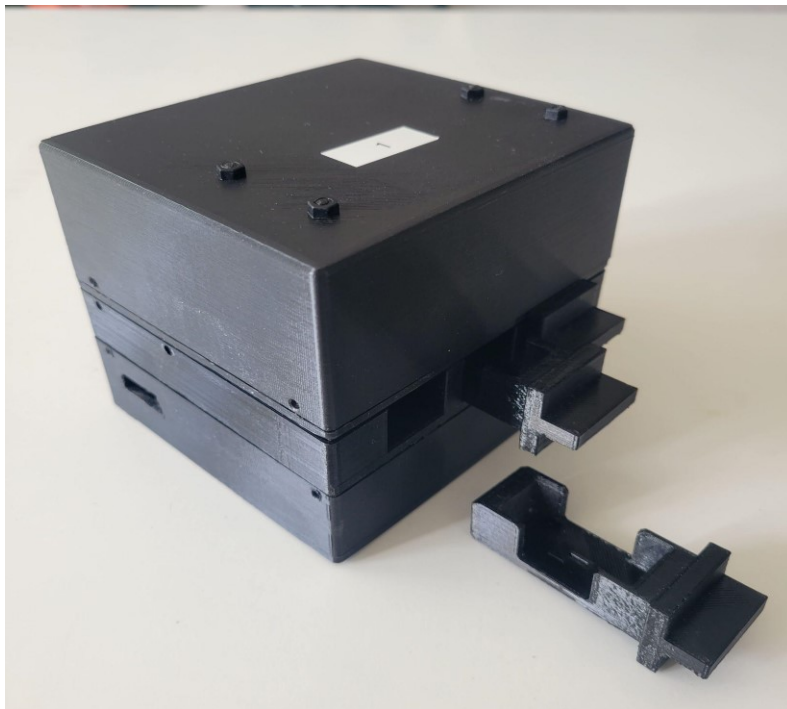
Figure 2.2. Revised 3-well sensor platform design with exposed cartridge tray

With the changes made and the 96-well plates deemed no longer suitable for containing samples, a custom fluidics cartridge was designed to work with the new sensor platform design. Figure 2.2 shows the revised sensor design that only uses three sensing slots and the tray used to hold a cartridge.

2.3.1 Refined PCB designs

New Circuit boards addressed issues that we initially experienced with the 96-well sensor platform device and worked to solve as many of these issues as possible. The dimensions of the PCBs were reduced to fit only the required parts, which helped to reduce the footprint.
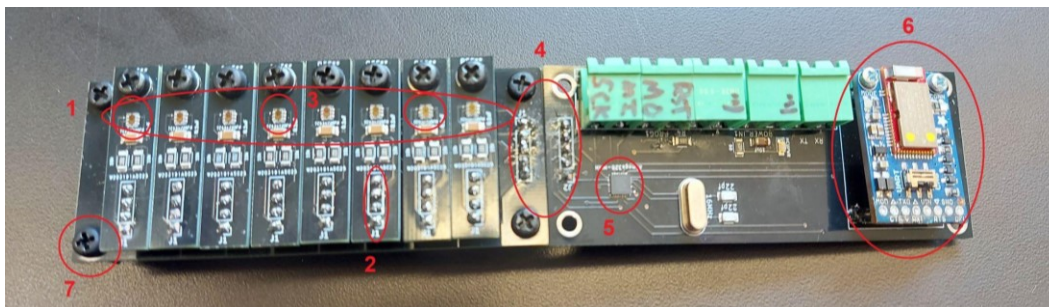
Figure 2.3. Combined MUX board and MCU board

Shown in figure 2.3 is the combination of the combined MUX board and Main board. There are eight small sensor boards that each contain a TCS34725 color sensor chip(element 1). This part was purchased online from Digi-Key Electronics. Individual sensor boards are attached to the MUX board through a soldered connection and use a straight-line formation(element 2). The eight individual sensor boards have a relatively small form factor hence they are spaced out according to a singular column on a 96-well plate, but for the 3-well sensor device, only three slots were used to mount the sensors(element 3). The MUX board is now attached to the main motherboard through a

5-pin connection instead of Arduino wires(element 4). The main motherboard houses the ATMega328P MCU(element 5) and the Adafruit Bluefruit Bluetooth Low Energy (BLE) chip(element 6) and has the same dimensions as the MUX board. Both the MUX board and the main board have 3mm mounting holes on the four corners(element 7), and the final assembly would have the two boards overlayed on top of each other and connected through the 5 pin connection while multiple 1 cm spacers(the equivalent of motherboard standoffs) are used on all four corners of the boards to secure the two PCBs in place. This assembly of the main board, MUX board, and multiple sensor boards will together be referred to as the sensing block.
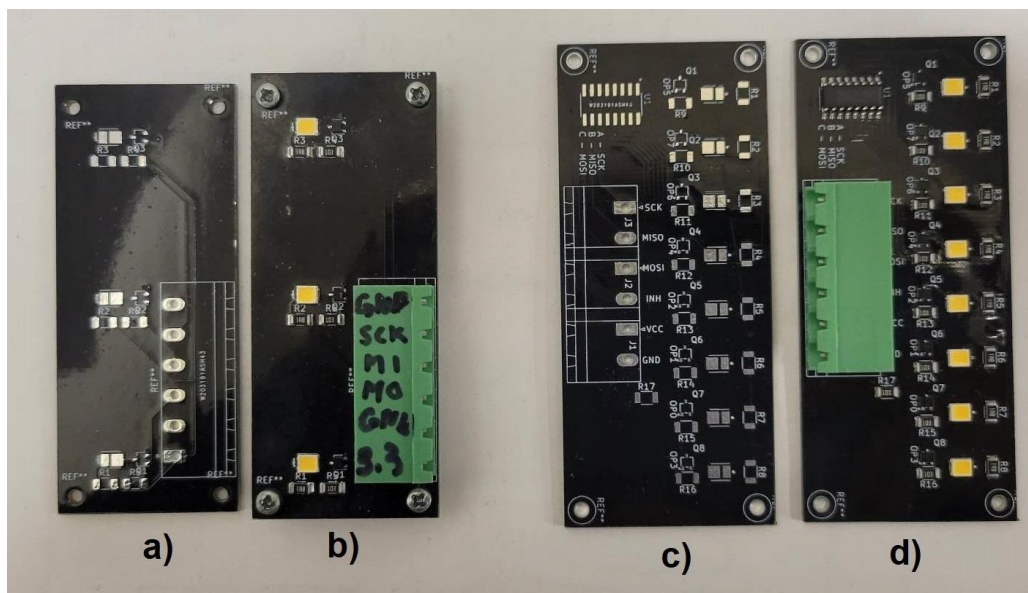
Figure 2.4. Lighting boards: a)Blank 3 light PCB, b)populated 3 light PCB, c)blank 8 light PCB, d)populated 8 light PCB

The next block, the lighting block, only contains one PCB, the lighting PCB, which is shown in figure 2.4. There were two versions of the lighting board designed, one which is similar to the previous designs of the 96-well sensor's LED board, shown by the PCB in figure 2.4(d). It is composed of a singular 3x8 MUX and eight white LEDs in a line formation, spaced out the same as the eight sensor boards. The other version of the PCB

is shown in figure 2.4(b); there are only three LEDs with no MUX required. Either one of the three light PCB or the eight light PCB can be used in the 3-well sensor device, the eight light PCB has the advantage of upwards compatibility with an eight sensor setup, but the 3-well sensor device only requires three sensors and three lights to operate. The mounted LEDs are positioned right underneath the sensor chips. The main board has three pins that control the LEDs, which are connected using phoenix connectors and stranded wires.

Figure 2.5. Populated Power board

The last assembly is the power block shown in figure 2.5, which contains the USB-C breakout board and the power board. This power block provides power to both the lighting block and the sensor block. Again, the connections are made using phoenix connectors and stranded wires. The output of the power board has two rails of 3V3 and 5V power, but currently, only the 3V3 power rail is used throughout the platform device.

2.3.3 Refined sensor device layout

The device casing is 3D printed using black PLA filament on a Prusa MK3s FDM printer. The layout of the three-well sensor platform took the same design approach as the 96-well sensor in that it is still a sandwich design, but the change is that it has only three layers.
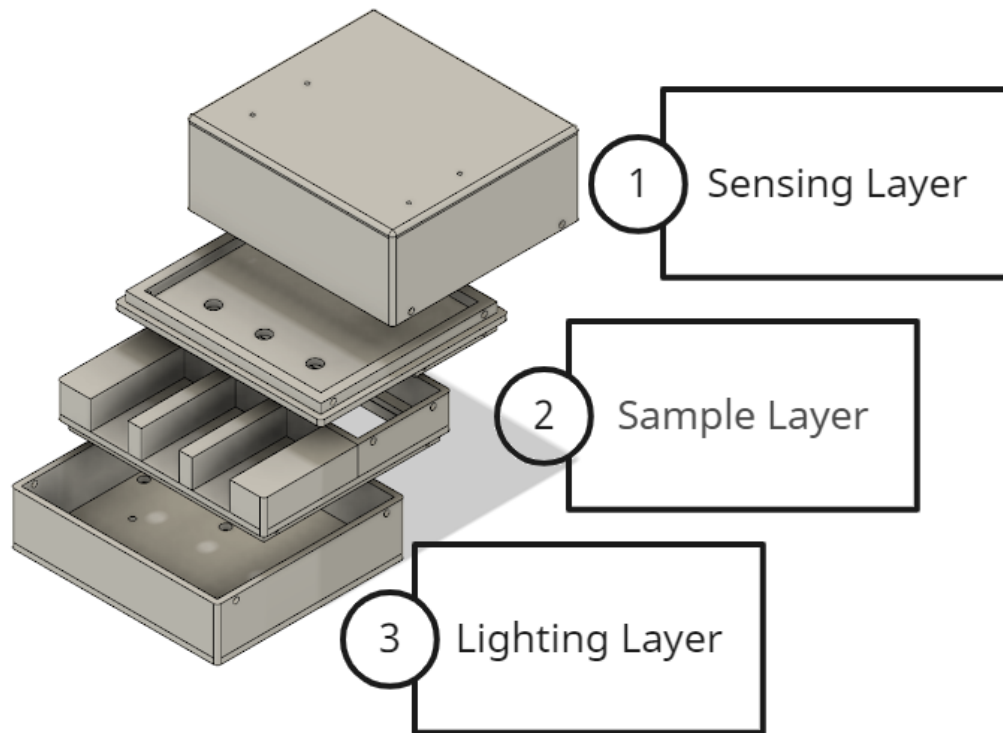
Figure 2.6. Fusion model of the device casing used for 3D printing

Shown in figure 2.6, starting from the top down, is the first layer of the sensor platform containing the sensing block assembly. The four corner holes used for spacers between the MUX board and main board allow for the screw ends of the spacers to protrude out and be connected to another spacer in series, this is then used to mount the sensing block to the lid of the device. Once mounted, the sensors are facing face-down

towards the allocated circular cut-out in the middle layer. An assembled view of the first layer is shown in figure 2.7.
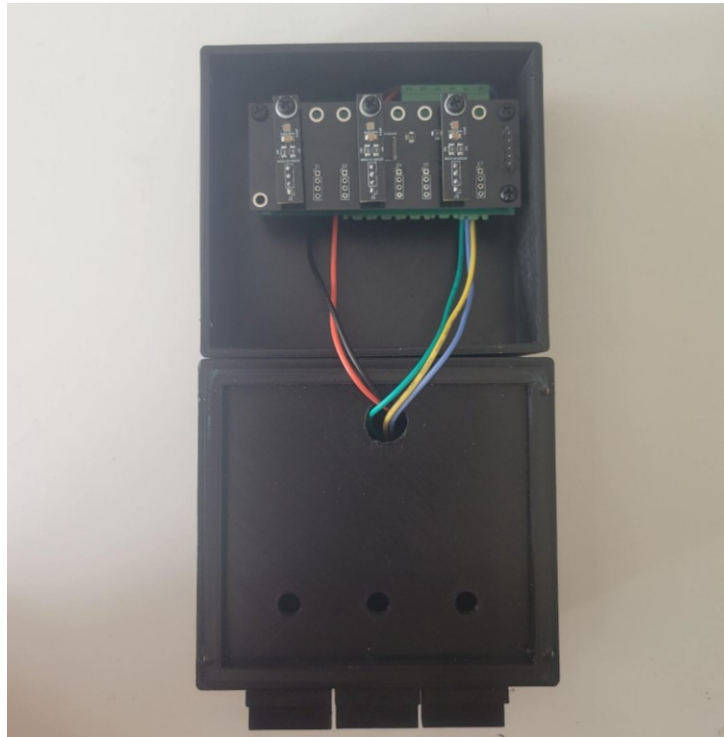
Figure 2.7. The physically assembled top layer of the 3-well sensor with three sensors mounted.

The middle layer of the sensor platform is made of two pieces and functions as the sample holding layer. As shown in figure 2.8, three total slots are cut out, one for each sensor in the top layer. The slots allow for a tray to be inserted. The trays hold the cartridges used to contain the samples for measurement.
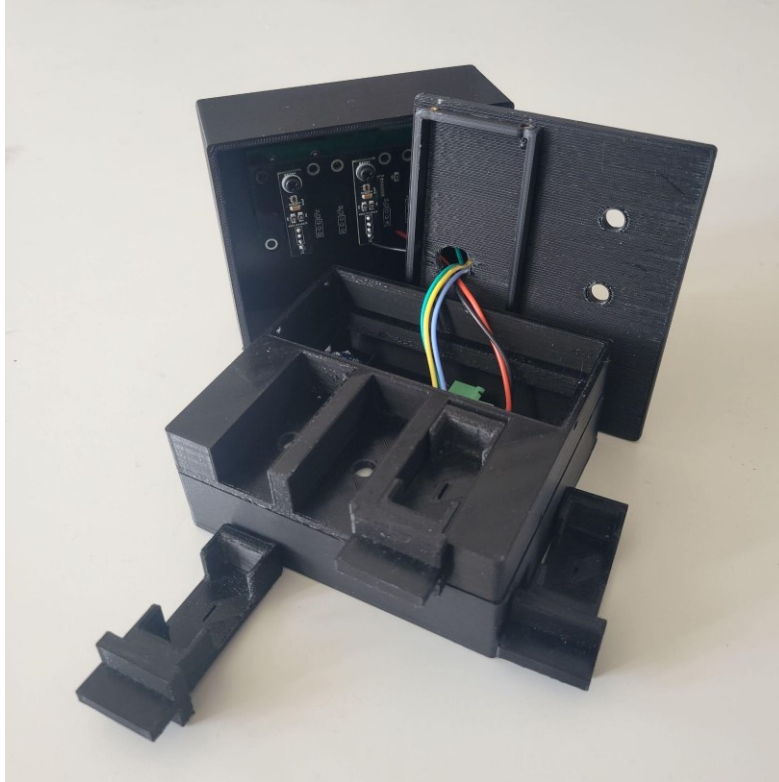
Figure 2.8. Physical assembled mid layer of the 3-well sensor with cartridge trays

In each slot, a vertical through hole 7 mm in diameter was cut at the location where sensors are located, and the tray used to hold the cartridge also has holes cut out in the same alignment.
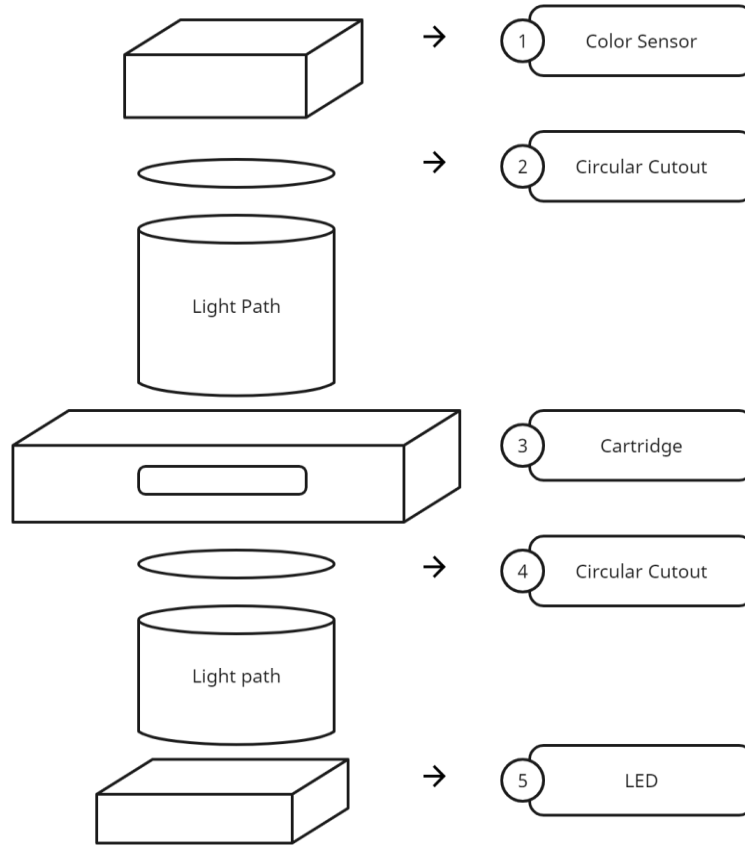
Figure 2.9. System Light path diagram

Shown in figure 2.9 is the model of the light traveling through the system. The unobstructed line of vision allows for lighting to travel from the LED in the bottom layer through the samples and directly interact with the sensing elements.

Figure 2.10. Physical assembled bottom layer of the 3-well sensor with a three LED lighting board installed

The bottom lighting layer is shown in figure 2.10, it contains both a lighting block and a power block. Similar to the sensing block, the two blocks in this layer also have mounting holes that are used to mount themselves onto the bottom casing of the device. The power block is mounted against the left wall of the sensor platform where a small slot allows for access to the USB-C connection, but is not so big such that ambient lighting conditions would affect the output of the lighting block. The lighting board was designed such that the LEDs are spaced exactly the same as the sensor slots on the MUX board, and this allowed us to easily mount the lighting board in the bottom layer and have the LEDs line up right under the three holes cut out for sensing.

2.3.2 Cartridge design

Since the new design of the sensing platform is supposed to work with only three sensing slots, the two choices would be to use only 3 out of the 96 wells in a 96-well plate or to design a custom well that can hold fluids for sensing. The first option requires the platform to have a slot that is big enough to fit the 96-well plate as well as some procedures to clear and clean the 96-well plate after every use, and there also exists the issue where sample volume difference can affect results. The second option can offer designs in the form of individual disposable wells that take up much less space and eliminates the task of cleaning. Additionally, the channel is designed so that minor variations in fluid volumes will not affect the measurement results since the measurement is taken using a portion of the total volume. The choice was to go with the second option while allowing for possible device adaptations to accommodate the first option.

In order to produce a disposable fluidic holding well that we can use in the 3-well sensor device, we need to keep the cost to manufacture relatively low while at the same time having high light transmittance and good optical clarity properties. We designed a cartridge that uses stacks of thin acrylic sheets with channels cut out in the middle layers, and these layers are then stacked on top of each other to create a fluidic channel. The channel has a set height, so there will not be any issues with varying fluid volumes affecting the optical path length of the sample. Also, only a small section of the channel is used for sensing, and the user must ensure enough fluid to cover up the sensing zone. The different layers were then sealed using weld-on acrylic glue to form the final cartridge.
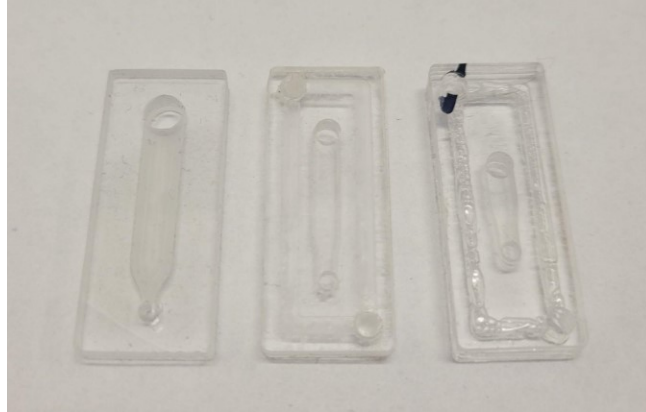
Figure 2.11. History of the Metabolite fluidics channel

Figure 2.11 shows the evolution of the cartridges. The initial cartridges were first designed to be made from three layers of acrylic, where only the middle layer had the microchannel cut out; improvements were made to assist in the manufacturing process so we could easily assemble the cartridges. This design proved to be an issue since three layers offered shorter vertical channel height, which meant low optical path length, making it easier for the color of the sample to be saturated by the bright LEDs.

Most of the problems encountered and solutions implemented were to address the optimization of received light in the sample. Due to the limitation of the assay, the total volume within the microchannel had to be kept at 100μL, meaning if the depth of the channel were to increase, then the length and width of the channel would, in turn, have to decrease as well.
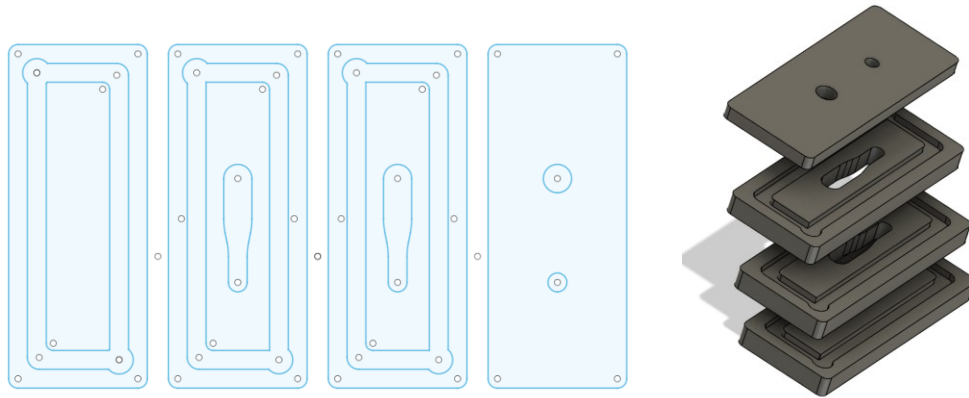
Figure 2.12. 2D & 3D design(Fusion 360 model) of the four-layer cartridge design

The designs shown in figure 2.12 is the improved cartridge model, four individual layers of acrylic are stacked into a cartridge. The channel created by the cutouts in the middle layers measures around 12 mm in length and 3 mm in height; it is irregularly shaped but measures 3 mm at its widest part. We have designed it to be top filled using the two exposed holes on the top layer, which acts as the inlet/outlet. The sensing zone is centered on the channel and only occupies 5 mm from the total length. Other than the top layers, the rest of the layers all have guidance channels to assist the flow of the glue when pressing the layers together, and this will help ensure that glue is not entering the channel. Based on the existing assay color reactions to be tested, the final volume of samples was set to be 100 μL; therefore, we have made sure that the channel of the cartridge has the ability to hold at least 100 μL of fluid while also providing enough optical path length for the color of the sample to be measured on the color sensor.

The cartridges were cut using a CNC (Computer Numerical Control) machine (model: D-11 miniTron) purchased from Cancam, and this device uses a computer-generated G-code to program the drill bit to mill down the material to its desired shapes. The materials we had access to were cast acrylic and extruded acrylic, and both offered

excellent optical clarity. Extruded acrylic is less expensive, but requires a different manufacturing method than what we had, so we chose cast acrylic.

During the quality check process after the manufacturing step, we noticed an issue with inconsistent layer heights, and this would theoretically affect the optical path length of the light that passes through the sample and cause measurement to be inconsistent when measuring the same sample using different cartridges, this is also the initial problem the new design was trying to address. After researching into the manufacturing process for cast acrylic, it requires the molten acrylic to be poured into a mold and left to settle before obtaining the final product. This process is known for creating subtle differences in thickness throughout a single sheet of cast acrylic. Ideally, a single cartridge made from 4 layers of acrylic should be 6.00mm in height, but using calipers to test the first batch of cartridges, I was able to measure out individual cartridges that range from 6.7mm to 5.2mm in height.

The issue was noticed in the later stages of the manufacturing process, as more than 200 cartridges had already been made. The plan was to try and salvage as much of the produced cartridges as possible, therefore, testing was done using two of the selected cartridges with near maximum and minimum observed height to determine how much the measured color results would vary when measuring the same colored sample solution. The test was done using colored water as the sample solution, and the results were collected using the sensor 0 on the reference sensor device, with a nearly 1mm difference in optical path length, the two cartridges measuring the same sample showed less than 1% variation in color. This result likely occurred due to the near 92% transparency of the acrylic material and the method by which the data was processed. If only the raw values of the sensor measurement were taken into account, then the observed color values would

be lower for the thicker cartridge as less total light passed through, but once converted to a percentage value (which is what is used in the later calculations), the results did not yield a significant difference.

However, the results were affected by the change in the total volume of the fluidic channel. Under the intended circumstances, the cartridges were designed to hold a minimum of 100μL of fluid, and this would be enough to cover the entire sensing area, but when the sensing area stays the same in the 2D plane while the z direction expands, the total fluid needed to cover the entire channel also increased, this is shown in figure 2.13.
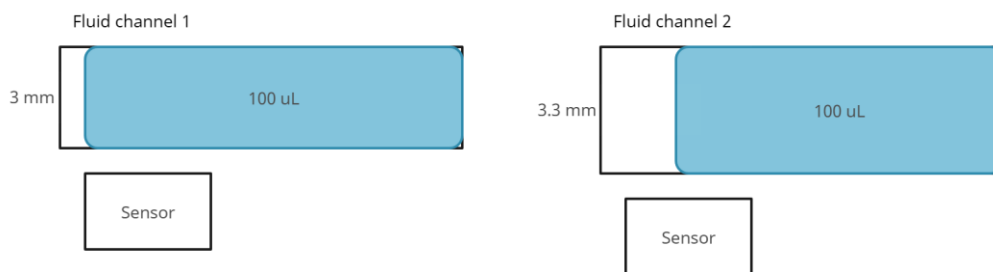
Figure 2.13. Comparison of different-sized fluidic channels and how it affects the fluid within.

After further testing by underfilling a standard cartridge of 6mm in height, I have determined that once the volume of the inputted fluid is below 90% of its intended volume (inputting 90 μL), the result would become affected, and at 60% (60 μL), no results can be obtained.
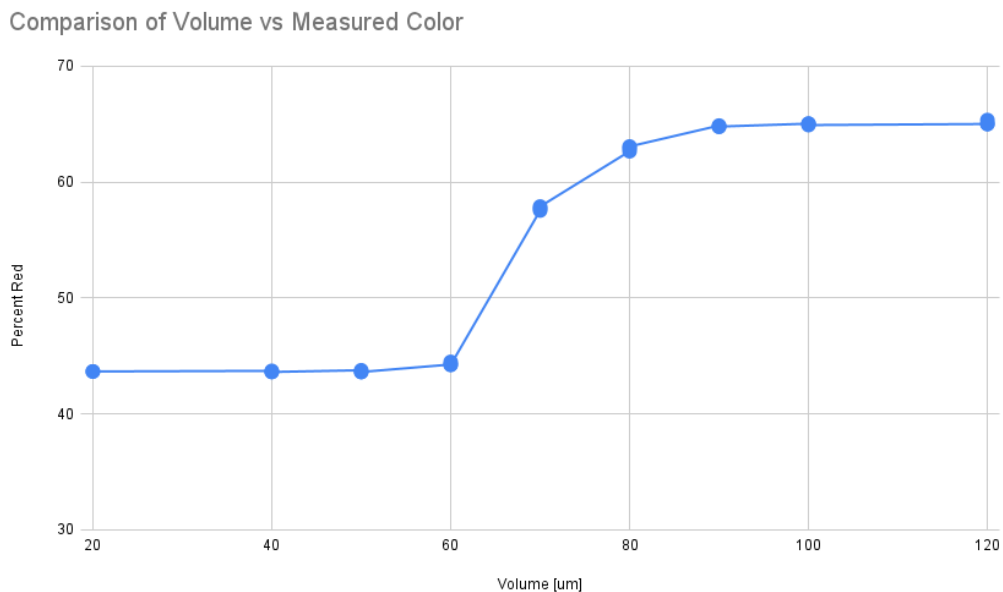
Figure 2.14. A plot of measured red value percentage in the underfilling cartridge test conducted with the same sample on the same sensor

The plot in figure 2.14 shows the measured result of underfilling the cartridge from 100μL to 10μL using the same sample. The measurement starts to become affected when the contents of the metabolite cartridge drop to 90% of the intended amount.

As a necessary precaution, we will set the cutoff threshold to be 90%, and through basic calculation of volume, we can see that if the height of the channel increases to 3.33mm, then 100μL will fill the channel up to exactly 90% of its maximum capacity. From these results, I decided it was necessary to reject the cartridges that are thicker than 6.3mm. On the other hand, overloading the cartridge will not affect the results at all, but could potentially cause a mess that requires users to clean up. Therefore, cartridges that are thinner than 5.7mm will also be filtered out in the quality control process.

Cartridge production was revisited further down the timeline when we ran out of the original batch that was produced, but this time we had access to better tools and learned from all the difficulties I encountered, so improvements were made. Originally, cast acrylic was selected because it could be manufactured using a CNC machine, whereas extruded acrylic could potentially shatter when subjected to the drill bit on the CNC. Now with the help of a PLS6.150D CO_2 Laser cutter from Universal Laser Systems(ULS) offered by the ELKO Engineering garage here at the University of Alberta (figure 2.15), we are able to make use of extruded acrylic, which has a more uniform layer thickness due to its manufacturing process. Also, using the laser cutter shortened the manufacturing time significantly.
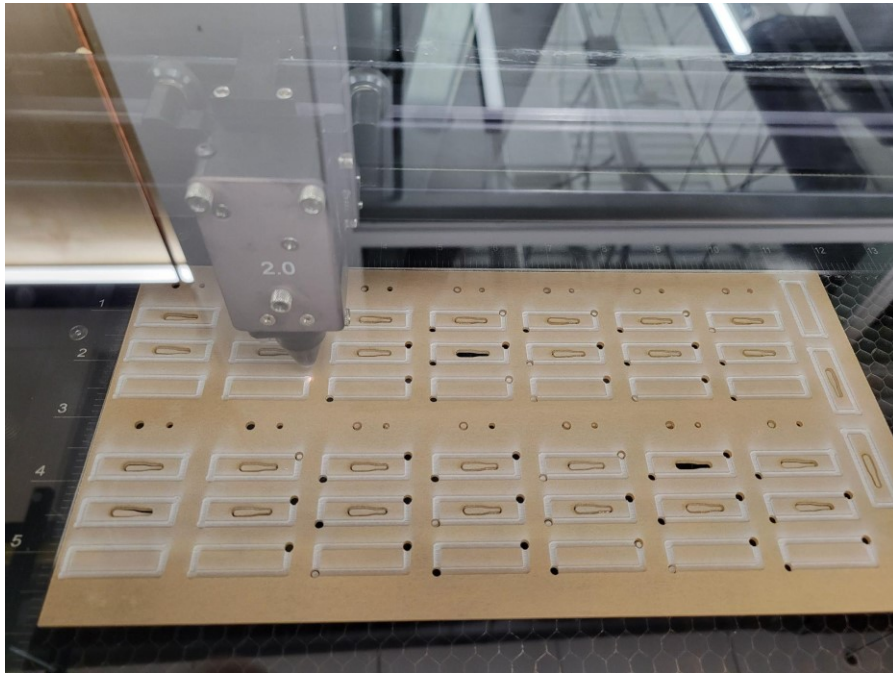
Figure 2.15. PLS6.150D CO_2 Laser cutter in ELKO Engineering garage cutting cartridges

2.3.4 Effects on manipulating lighting conditions

The design of the sensing platform has the SPMWH1228FD LED positioned vertically in line with the channel of the cartridge and also the TCS34725 color sensor while being spaced 1.5cm apart from each other. The LED outputs white light that has a luminous flux as high as 6500K, without ways to diffuse or reduce this light source, it became very problematic for the sensor to measure any samples since the resulting light, after passing through the cartridge layer, becomes saturated due to the overpowering white light. This issue was evident when the sensor reading for different samples all came back to be around 65000 in terms of alpha value, which was near the upper limit of 65536 (16-bit binary number), the calculation aspect will be further discussed in chapter 3.

As the first step in trying to solve this problem, layers of diffusion paper, purchased from staples, are used to scatter the light output of the LEDs in hopes of making the lighting more evenly distributed.
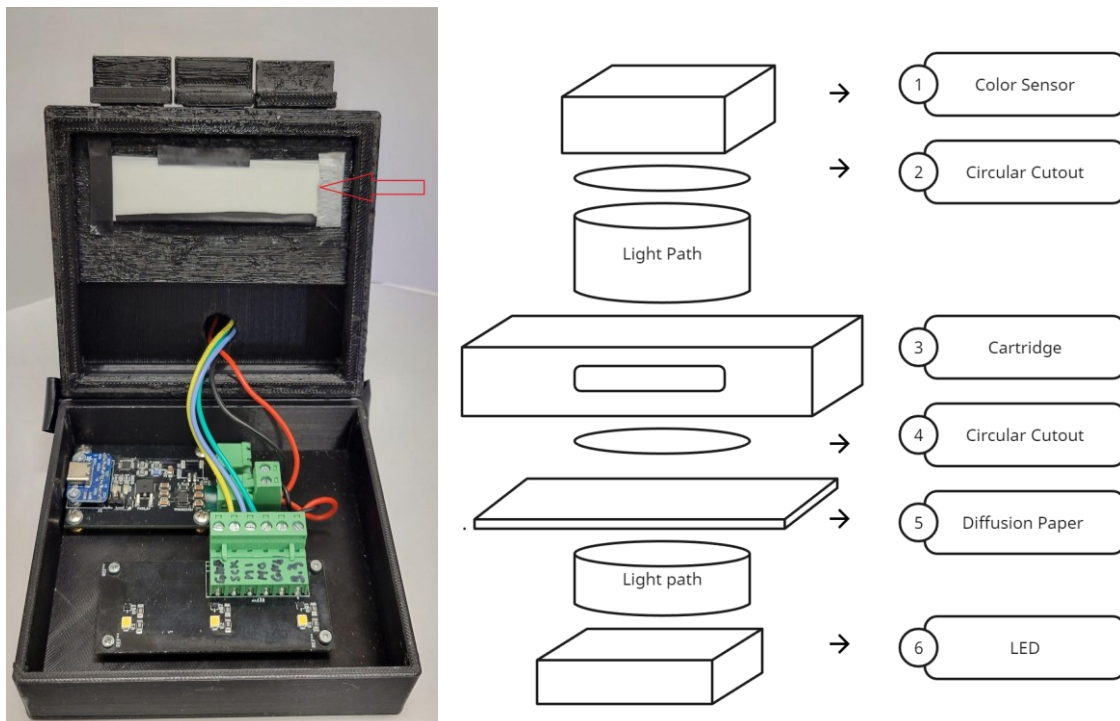
Figure 2.16. New system light setup with diffusion paper implemented and light path diagram

The final setup uses four layers of diffusion paper taped to the middle layer casing right above the LED as shown in figure 2.16.

The next step taken was reducing the background light received by the sensor from the ambient lighting condition. We have already made the environment into a black box condition through the design of the sensing platform, and now we just have to concentrate the lighting such that any light that the sensor receives will have traveled through the channel in the cartridge already. The original setup we used was a 7 mm hole from the light to the sensor, but since the shape of the channels will not be able to completely cover up the hole, the light that leaks through the two sides of the channel will cause the observed sample color to be saturated as well.
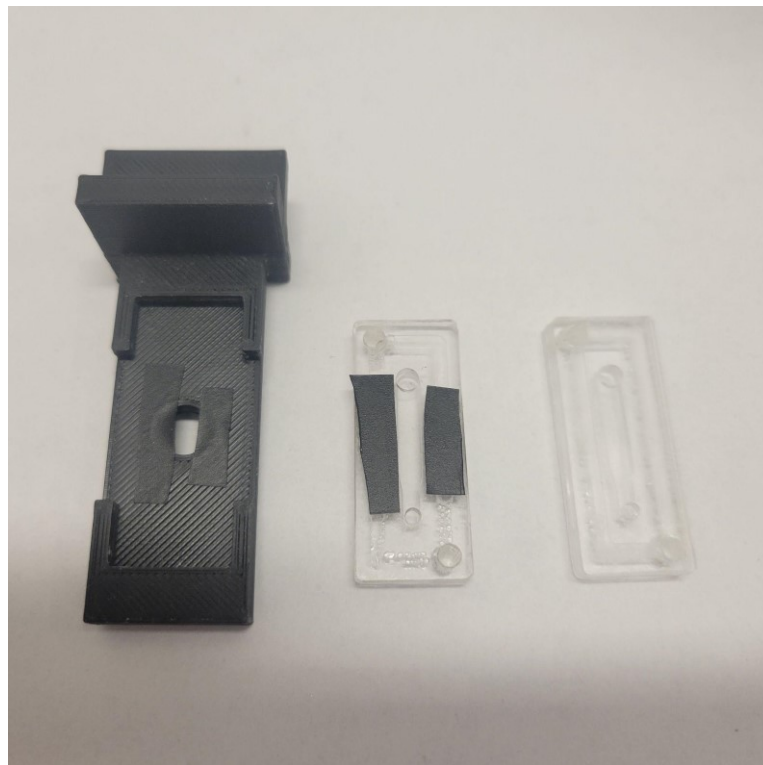
Figure 2.17. Adaptations to Cartridge and Tray for improved resulting light

The solution I came up with (figure 2.17) was to change the design of the cartridge tray to one that has a rectangular slit instead of a hole. The dimensions of the slit required further testing and adjustments, but when combined with the diffusion paper, it effectively eliminated the saturation of sample color and brought down the alpha value to the hundreds and thousand range.
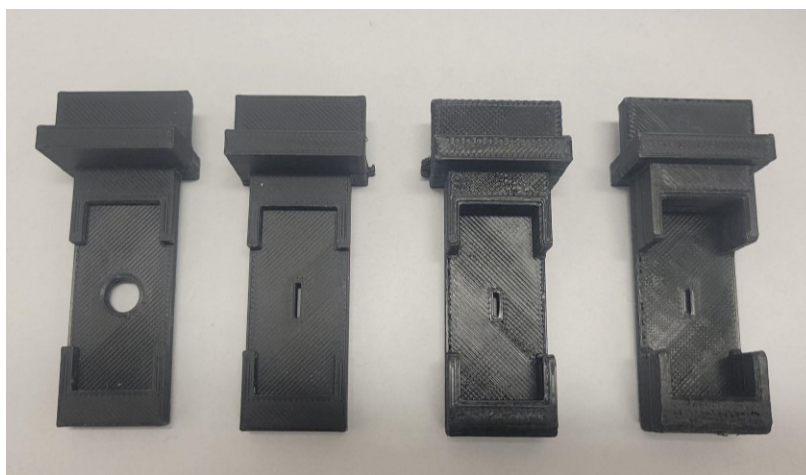
Figure 2.18. Evolution of the cartridge holders.

Figure 2.18 shows the attempts at changing the size and shape of the cut-out from circular to rectangular slit.
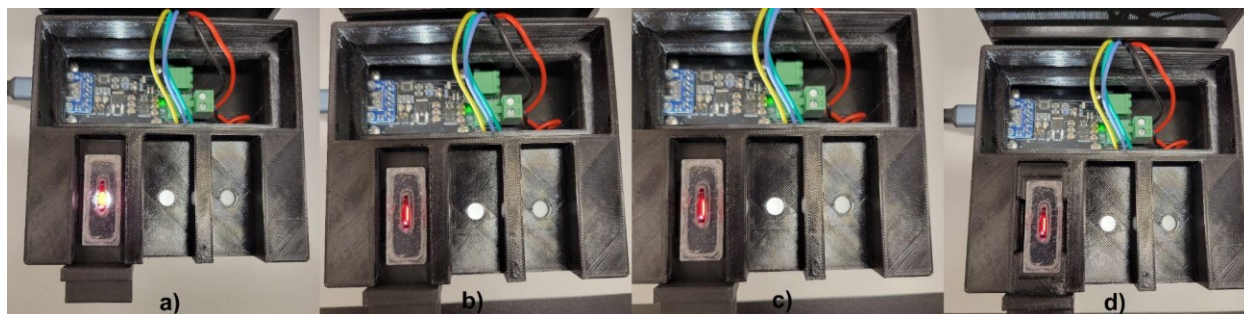
Figure 2.19. Result of the cartridge evolution.

Figure 2.19 shows the resulting light when measuring the same sample. The resulting alpha value stabilized at the 1000 range since white light did not spill out from the side of the microchannel where the samples were kept.

Chapter 3

Android Controller Application Design

Analytical chemistry usually needs experimental data to be collected and processed before analysis. If the diagnosis requires the combination of multiple sets of data before analysis, then there will be some form of data organization and processing needed.

We, as a team here in the Tricca lab, believed the best approach to creating a portable and affordable Point-Of-Care sensor platform device is to have a physical sensor device that acts as a receiver device while having a separate Bluetooth capable android device that will serve as the controller to control all its actions. All the commanded issues to the device will be sent over Bluetooth Low Energy (BLE), which is a Bluetooth communication variant, and no physical button will be available to control it. Similarly, all data collected on the device is sent back to the android device upon request through Bluetooth as well. An android application is created just for this purpose. The app can send commands, receive data, save the data, process the collected data using pre-programmed functions, and finally, provide the necessary analysis of the obtained data.

The android application has multiple versions, and each has undergone numerous countless revisions. Each version of the application is catered to suit different needs, such as operating a new version of the sensor or streamlining the process for the end-user.

The three versions of the application discussed in this chapter include the Clinical data collection application, which is the first application designed to operate the complete process, this user faced application was challenging to test and debug, so the next

application was created. The Central sensor control application was a purely developer-facing application that allowed developers to quickly and easily test every aspect of the sensor device. Finally, the official test application was created using the groundwork from the first two applications; it is strictly for the user and will allow an operator with limited experience to conduct the complete assay process.

With every version introduced, there were also numerous revisions to improve the end-user experience and bug fixes. The end goal of the project is to create an application with the following functionalities: each user will have their own personalized profile whose data is encrypted, and the user can update their current health information that is related to the metabolite test and save it as part of their records. The application will have the ability to control the functionality of the physical sensor device over BLE and then receive the measurement data sent back to the application from the sensor through BLE communication. For our purposes, using the lower data transfer rate of Bluetooth Low Energy was enough, and it can also reduce power consumption compared to regular Bluetooth. After each measurement, the resulting data obtained from the tests done on the sensor platform will be logged into the records of the user and saved as part of their records. The application will be able to combine the results from the test together with the recent health record of the user and provide the user with feedback on their current health condition. The application will be preloaded with calibration curves and reference standards to assist in the data processing aspect. The weighted average of the measurement will be used to determine if the threshold is exceeded. If so, the user will be notified that they should seek professional medical diagnostics.

3.1 Clinical data collection application

The clinical data collection application was the first version of the application I had created to operate the device, and it was initially designed to be a complete app that would take into account the clinical data as well as the sensor measurement data in order to provide the user with a final diagnostic result.

The first step was to create an android application using android studio, this version of the application was to be used on modern smartphones and tablets with Bluetooth functionality. At the time of creation, this version of the application was installed with the most up-to-date Android version, Android Q, which is the 10th version of the Android operating system. The application was also programmed to have backward compatibility up to android Oreo, also known as android 8.

A basic android activity consists of the following components. An activity, which is like a window for that application to display its user interface. The layout, which is associated with an activity, is the design of the user interface. Elements within the layout are called views. Classes are templates used to create objects and methods, and activities are a type of class.

In this application, there needs to be a separate activity for each of the functions outlined in the requirements. A login activity that took in one user input string as the username and another string as the password. Once past the login screen, the proceeding activity is a list of health-related information and questions the user had to provide. If the user has already entered this information, they can update it or skip to the proceeding step. The page of questions focuses on the following aspects, gender, birthday, smoking history, whether blood was observed in the stool, recent changes in the caliber of the stool,

changes in the consistency of the stool, the shape of the stool, and if there has been a rapid weight change in the user. These factors or a subset of these factors are specific to colon cancer, though other questions or clinical factors can be added or changed for other types of tests in the future.

Figure 3.1. Clinical factor activity screenshot

Shown in figure 3.1 is the screenshot of the activity, questions are placed in their own textbox, and radio groups are placed next to the textbox such that the associated answers to the questions are linked to each radio button within the radio group. This implementation ensured the user could select only one out of all the possible choices, as it was the main functionality of the radio group object. To obtain information regarding the date of birth of the user, a date-picker function was implemented, which lets the users

41

select the date and time from a list. To proceed to the next activity, the application checks over all the user inputs to ensure no mandatory question is left unanswered. If there is a missing input, the user is prompted to check over the page and answer any unanswered questions. At this stage, the user can move to the next activity when all the mandatory information is in place. Pressing the "NEXT" button will cause all the entered information to be saved within the app.

The next activity was planned to have the capability to send measurement commands over BLE, and collected data from the sensor were to be transmitted back to the application through BLE, these data will be combined with the patient health data and saved into a comma-separated value (CSV) file in the internal storage of the Android tablet, this human-readable file can be accessed in the Android tablet by the user.

Due to inconveniences when using this version of the application during testing, the development of this version of the application was put on hold at this stage of development. The major setback of this application was the inability to quickly navigate to the BLE command output activity, which slowed the overall testing process. This happened due to the application locking access to the next activity unless all information was filled out; this included the username, password, and all user health information.

3.2 Central sensor control application

The newly developed version of the application was given the name "Central-Sensor-Control '' (CSC), and the design philosophy behind this version of the application was to create a developer-only control panel that gave access to all functions in one compact screen layout, with as few restrictions as possible, this can be seen as an

improvement which benefits only the app developers. As a change from the previous version, this version of the application did not have a login activity but instead had a singular "START" button on a blank activity that took the user to the Bluetooth connect screen. Since Bluetooth setup was a one-time process, having it separate from the main control screen will help save room for more buttons and a display area, the screenshot of the activity is shown in figure 3.2.

Figure 3.2. Bluetooth activity screenshot

3.2.1 Sensor command

The application sends commands by sending 8 character long strings, the first character interpreted by the sensor device is used to set the command, while the rest of the characters provide information for the command being issued. Please refer to the below graph for the functionality of each command.

43

Sensor Command initializer	Functionality
"S"	Set timer for measurement
"R"	Reset timer for measurement
"D"	Send stored data
"F"	Setting flag

Table 3.1. BLE commands.

The second character in the "S" type sensor commands specifies which specific color sensor on the device is going to take a new measurement. The eight sensors are addressed as "S0, S1, S2, S3, S4, S5, S6, S7". The remaining characters represent a millisecond time value which is used to set a timer before sensor measurement. For example, if sensor three were selected to be measured in 2 minutes, the command sent would be "S3120000". The "S" represents the "Set timer before measurement" command, the next character "3" represents which color sensor we want to take the measurement, and the remaining characters, "120000", represent the millisecond value of 2 minutes. The "S" header was the only type of command to make full-use of the maximum number of characters in the string.

The "R" type command is used for resetting an active timer. This header is followed by a single number indicating the sensor number. E.g., sending "R3000000" before the 2-minute timer ended in the previous example would stop the timer and cancel it. A reset is useful in the case of a user improperly following instructions and needing to restart the test. Since memory on the responder device is limited, this command also helps to save the most recent valid measurement.

The collected data from the sensor is programmed to be automatically sent back to the application after each measurement instance (after each "S" command). Still, in rare instances, this data can be lost, so as an added safety measure, the "D" type commands are used to request the data that was previously recorded on a specific sensor by pairing the "D" header with a second character that indicates the sensor number. E.g., sending the command "D3000000" would retrieve the measurement data taken using sensor 3. If the controller and the receiver device ever lose connection between a command and a measurement, this command ensures that no data is actually lost.

The "F" type command is a special flag used to distinguish between sensor devices used for testing. When the second character is "0", the sensor device will operate in 96-well sensor mode, and a "1" will allow the sensor to operate in three-well sensor mode. The main difference between the two modes is the performance of the LED PCB. When the 96-well sensor mode is activated, the 3 Arduino pins connected to the LED PCB operate in binary logic mode. This was done so all 8 sensors on the sensor platform device could be used in different applications. Otherwise, this project used only 3 of the 8 available color sensors. A detailed truth table for the 96-well mode is shown in table 3.2.

Pin 0	Pin 1	Pin 2	LED mode
0	0	0	S0 LED ON
0	0	1	S1 LED ON
0	1	0	S2 LED ON
0	1	1	S3 LED ON

1	0	0	S4 LED ON
1	0	1	S5 LED ON
1	1	0	S6 LED ON
1	1	1	S7 LED ON

Table 3.2. 96-well sensor device LED truth table

Pin 0	Pin 1	Pin 2	LED mode
0	0	0	OFF
0	0	1	S0 LED ON
0	1	X	S1 LED ON
1	X	X	S2 LED ON

Table 3.3. Three-well sensor device LED truth table

The LEDs in the 96-well sensor design utilized a MUX to control the output, and the off condition was determined using an external enable pin. The three-well sensor LED activation methods are outlined in table 3.3.

3.2.2 Measurement properties
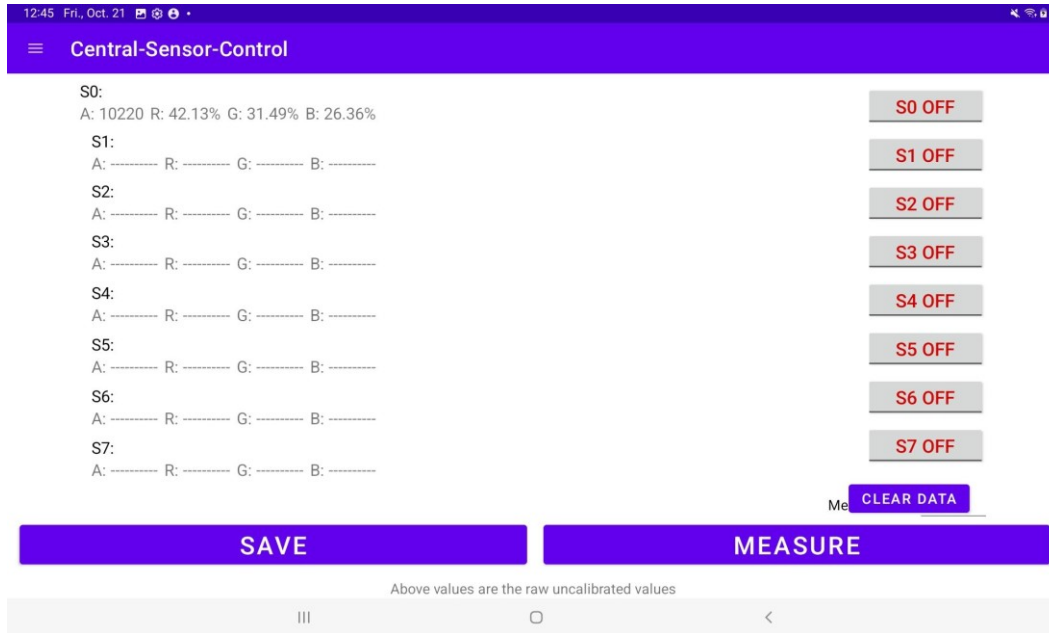
Figure 3.3. Central sensor control application main controller activity screenshot

Shown in figure 2.3 is the layout of the main activity. The majority of the screen space was reserved for displaying data, and the eight toggle buttons on the right of the screen control which sensors are measured when the MEASURE button is pressed. Default settings initialize all sensors as off. The four buttons on the bottom of the screen governed the data collecting, saving, erasing, and processing steps of the application. The EditText object at the bottom right of the screen above the measure button controlled the measurement overtime function.

The user would operate this activity by first identifying which sensors are used, then toggling the button for that sensor from "OFF," indicated by the red color text, to "ON," indicated by the green-colored text. This action will toggle the associated flag variable within an eight-element array that indicates the sensors to be measured. Next, the user would identify what type of measurements are to be taken. If the basic one-time

47

measurement is required, then pressing "MEASURE" will suffice, and the associated timers for each sensor are set to zero for the purpose of efficient testing (e.g., "S1000000" is sent for sensor 1). When the onclick method is initiated, the code enters a loop that checks through every element in the flag array, indicating which sensors are to be measured. If the flag check returns "TRUE," then the measurement for that specific sensor is taken, and the code will iterate through the whole array until all flags are checked. The onscreen textboxes are updated with the measurement results when the BLE communication process is complete, and data is then sent back to the tablet. However, if the required measurement is to observe the change in samples over a period of time, then the measurement over time function is used. First, sensors to be used to measure the samples are selected. Second, an integer time value (in seconds) is entered for the period these samples would be observed. Lastly, the "MEASURE" button is pressed, and the process is completed after a short wait. Note that the onscreen text box will only be updated with the last measurement, but the complete data set is saved within the application.

Measurements are taken in sequential order, meaning if sensor 0, sensor 1, and sensor 2 are all selected, the measurement would first occur on sensor 0, and sensor 1 measurement process will only be started after the LED protocol is completed and the BLE communication protocol is finished. This BLE communication protocol is rather quick and would only take ~700 milliseconds per measurement, but the LEDs require a small waiting period before measurements can be taken, this is due to the power-up delay property of LEDs. The LEDs used in this sensor device react quickly to power but require ~300 milliseconds to get to maximum brightness, so to ensure measurements are taken under consistent lighting environments, a delay of 1000 milliseconds is added before each

sensor measurement after the LED is turned on. LEDs will stay on for the whole duration of the measurement, which requires 1000~2000 milliseconds, this variability in measurement time is due to the implemented fault tolerant procedure that is used to counteract the current fluctuation of the sensor photodiodes. There is a chance that the maximum value or minimum value is measured due to the current output of the photodiodes not stabilizing. As a solution, the sensor device will filter out any values that read 65536 (2^{16}) or 0 (2^{0}), and the measurement will be taken again, up to a maximum of 3 repeated readings. With these considerations, each measurement takes around 3 seconds to complete, and five measurements can be completed in ~15 seconds. Thus, when the user chooses to measure on multiple sensors over a period of time, the resolution will be lower compared to when fewer sensors are selected.

3.2.3 Data Processing

The data that is collected and transmitted from the sensor device is organized into 16 characters long, 64 bits in size, hexadecimal string, with an additional header character, resulting in the format "SAAAARRRRGGGGBBBB." Here, "S" is an integer value that indicates the sensor that the measurement was taken on, "AAAA" was a 16-bit hexadecimal number that represented the alpha value, and "RRRR," "GGGG," and "BBBB" represented the red, green and blue values, respectively.

This 17-character string is sent by the sensor device through Bluetooth after each single measurement instance and then saved by the Android application after each measurement is received. The Android application was set up to only process received data in the previously mentioned format, it checks the first character in the string to

determine which sensor data was received, and if anything outside of the integer range of 0-7 is received, the data will be ignored, and the application will return to standby. If the received data passes the first check, the next 16 characters are parsed into four strings of 4 character length, and these strings are then converted to integer values using Integer.parseInt() function.

Due to the inherent hardware differences in the photodiodes in different color sensor chips, sensor-to-sensor calibration was necessary in order to reduce the variability in measurement across multiple sensors. Taking multiple samples of increasing concentrations, measurements were taken using every sensor, and a single sensor was chosen to be the reference sensor such that all the other sensor measurements were manipulated to match the output of the reference sensor (More details can be found in Chapter 4.2.3). The calibration procedure resulted in a set of bias coefficients and offset constants that are applied to every measurement, and these values differ depending on the measurement sensor. When the received data is converted to integer values, these integer values are converted to percentages, then multiplied by the bias and added with the offset to produce the calibrated values. The application will save both the raw and calibrated values.

3.2.4 Data Storage

The application is initialized with 2 ArrayList of integer ArrayList objects (ArrayList<ArrayList<Integer>>) that can be accessed globally, one is used for recording the raw sensor measurements while the other is for the calibrated sensor measurements. Within each ArrayList, there are 32 integer ArrayList objects (ArrayList<Integer>); since each sensor requires 4 ArrayList for the alpha, red, green, and blue values, combining 8 sensors makes up for a total of 32 ArrayList. ArrayList objects in Java do not require a predefined size, meaning new values can be added to the list as long as the data type matches, this property makes it ideal for storing measurement data. The data collected in the ArrayList are cleared using the Arraylist.clear() function within Java libraries, and the "CLEAR DATA" button is used to activate this function. Note that using the measurement over time function will also trigger the clear function before the start of the first measurement. This implementation ensures that only the current set of test results is saved.

Data saving is done through the functions associated with the "SAVE" button. Within the onclick method, there is an initial permission checker that will check if the application has been granted permission to access the external storage of the Android device. If permission is not granted, the application prompts the user to grant the required permissions, else, the next command is executed. A CSV file is created in the device's "Documents" folder. This is a plain text file that contains an array of data separated by commas, mostly used for data storage and cross-platform access. The Java printwriter library is used to print data onto the output stream, and this stream is linked to the CSV file that was created earlier. The printwriter first iterates through the calibrated data

ArrayList of integer ArrayList, grabbing all the contents of the 32 integer Arraylists and transferring them to the CSV file, then the output stream is closed and the CSV file is saved with a name that is the current timestamp obtained from the system clock. This process is repeated with the raw data ArrayList of integer ArrayList, but the file name will have a "raw-" header added before the time stamp. The user can access the saved file by navigating to the file explore application on the android tablet, this file can be opened by Microsoft Excel for a quick inspection.

3.3 Official test application

This version of the application was designed to be the finalized user application that will accompany the newly designed 3-well sensor to be shipped to Nigeria and tested on real patients during validation studies. This application is able to provide a detailed set of instructions to users with limited to no experience such that they can independently run a complete test with 3 metabolite assays within a 30 min time period.
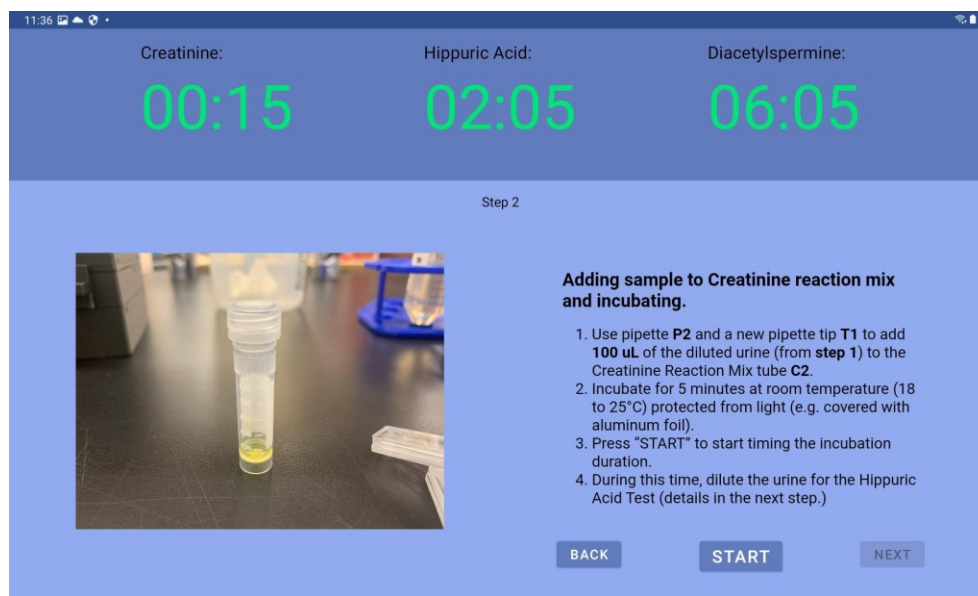
Figure 3.4. Official Test Application Creatinine assay tutorial step two screenshot

This application can wirelessly control the workstation designed to automate the three metabolite tests. Shown in figure 2.4 is the command screen for creatinine assay, pressing "START" will cause the tablet to send a delayed sensing command to the mounted sensor on the workstation device.
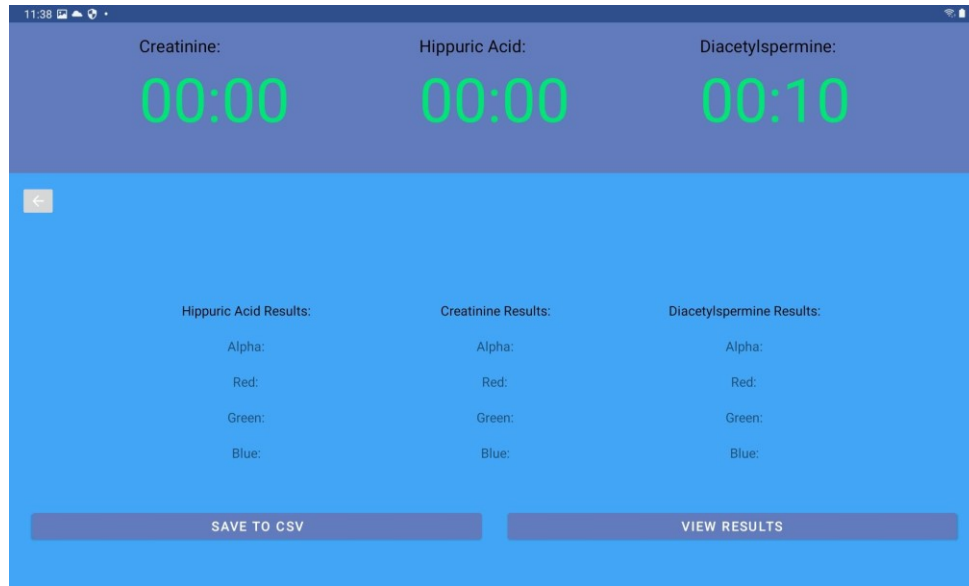
Figure 3.5. Official Test Application result activity screenshot

Finally, this application combines the results from the three tests (Figure 2.5) while considering the user-inputted clinical factors to provide positive or negative results for the CRC screening, as shown in figure 2.6. Furthermore, the results are also exported into a CSV file for record keeping.
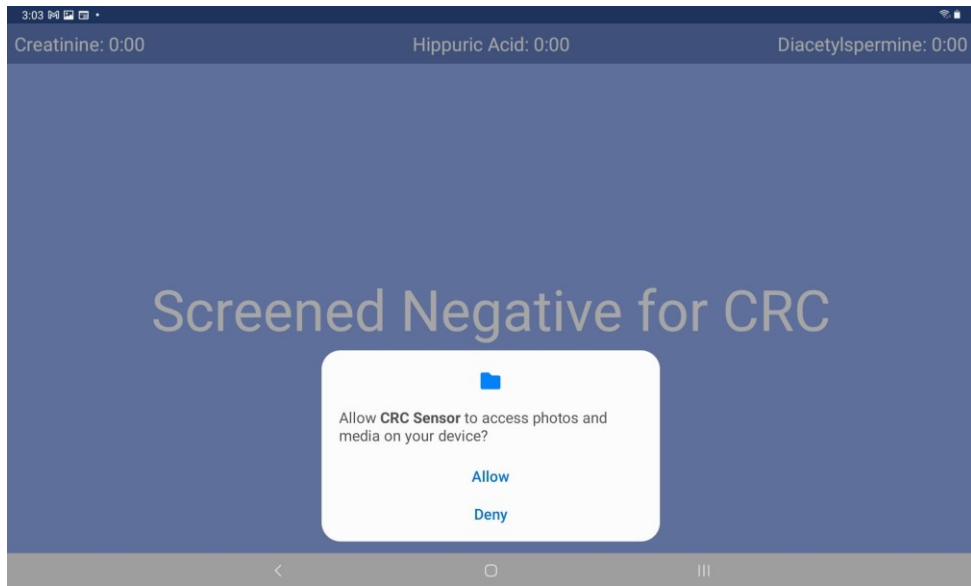
Figure 3.6. Official Test Application diagnostic screenshot

3.3.1 SQLite database

As an improvement from the previous data storage method, an SQLite database was created in order to move away from saving data to the ArrayList within ArrayList type objects. The advantages that were gained from this implementation included a more structured data storage method, and the measurement data is saved into the database as a single entry rather than across multiple array lists. This data is also more robust since content stored within an SQLite database does not get erased when the application is terminated or uninstalled, making the data more recoverable in the long term. Queries are used to access data within the database, this method offers more freedom than writing code that would iterate over specific array lists and copy specific elements into an output stream, and since each measurement is saved as one entry, there is no chance for any array size mismatch errors to occur.

The process to read from and write to an SQLite database occurs as follows. Upon initialization of the application, the application checks for the state of the existing database, if there is not a database, the application will create one using the predefined names and data class, this usually occurs on a brand new Android system with no previous installation of the application. However, if there is already an SQLite database created for this purpose, the application will grab an instance of the database and work with a copy of the database rather than the database itself.

A user-defined query was used to write data to the database. The query takes in data in a specific format and stores that data in a specified location within the database. When storing sensor measurement data, the default storage location is right after the previous entry. The application will check for the previous entry using the instance of the

55

database it has created and then make changes to the original database using the query. Reading the data stored within the database requires a "get" query that reads the desired contents within the user-defined scope; this can either be a "get all" or "get all with index." Applying the get.query on the database instance will create a Java list with the desired objects that have the same class as the database objects. The program then iterates through this list and saves every element within this list to the output stream; again, this output stream is linked to a newly created CSV file. Note that the SQLite databases created on Android systems are only visible to the application that created them. There is one copy of this database on the system, so any future write access to the database changes the original database. The content is automatically updated every time a change is made so that no work is lost in case the application crashes. Additionally, the Android default database SQLite package offers excellent source and target compatibility support, making the database suitable for future Android system updates. After finding success in this update, the CSC app was also implemented with the SQLite database feature for data storage.

3.3.2 Color number calculation

As a modification from the previous version of the application, the CSV data that is outputted from the application was changed to a single CSV file with raw sensor measurement values, calibrated color numbers, and concentration. The color number is a single arbitrary value used to represent a color, and the concentration value is calculated from the calibrated color number of the measured sample using predetermined curves.

The raw sensor measurements only contain red, green, and blue values, and in addition, yellow, cyan, and magenta values were extrapolated from the raw values to improve the accuracy of the color determination. The process begins with the raw values being calibrated according to the sensor-to-sensor calibration corresponding to the sensor used. Once the calibrated color percentages are calculated, the app takes the weighted sum of these percentages using the color number equation (Eqn 1). Depending on the assay tests conducted, the color weight will change to reflect the different color trends observed in the assay calibration curve. If a specific color had a higher weighting, it would indicate that it was the predominant color of the assay. Although the color number value holds no meaning on its own, it does allow for a quick and easy assessment of the measured results, also, working with one value instead of four is much more manageable.

$$Color\ number = \sum((\frac{color\ percent}{100}) * color\ weight) \quad (3.1)$$

$$Color\ percent(RGB) = (\frac{color\ value}{red\ value + green\ value + blue\ value}) * 100 \quad (3.2)$$

$$Color\ percent(YCM) = (\frac{color\ A\ value\ +\ color\ B\ value}{2 * (red\ value + green\ value + blue\ value)}) * 100 \quad (3.3)$$

$$Color\ weight = SIGN(slope) * ((1000000^{(\frac{|slope|}{100})} - 1) * (1000000^{R^2}) \quad (3.4)$$

The color number calculation is given by equation 3.1 where color percent refers to equation 3.2 and 3.3, equation 3.2 is the formula to calculate red, green, and blue color percentages. In contrast, equation 3.3 is the formula to calculate yellow, cyan, and magenta color percentages. Note that colors A and B refer to the combinations of any two

colors, yellow is red mixed with green, cyan is green mixed with blue, and magenta is red mixed with blue.

The weight of the color given by equation 3.4 depends on the in-lab calibration data collected for a given colorimetric assay, an example of this is shown in Chapter 4.3. In an ideal situation, the measured RGB values will increase proportionally with the increasing concentration of metabolite within the urine sample. If an assay has a predominantly red color trend, then the measured red percentage will increase while the other color percentages will decrease. This trend for each color is recorded, and polynomial regression is conducted to determine the slope and coefficient of determination(R^2), equation 3.4 converts each color trend to a color weight using these values. Note that this color weight will differ for each colorimetric assay since the observed color trends are different. Therefore, the range of possible color number results also varies from assay to assay (e.g., 500-1000 v.s. 5000-10000, more can be seen in Chapter 4).

3.3.3 Assay calibration curves

The obtained color number is associated with a calibration curve given the pre-knowledge of which type of assay was measured, and the concentration of the metabolite within the sample is obtained as a result. Calibration curves are obtained experimentally in the lab and relate known metabolite samples' concentrations to their measured color values. Depending on the type of assay, this relation can be linear or polynomial. Ideally, linear relationships between absorbance and concentration can provide the most accurate

results, but due to saturation at higher metabolite concentrations, the concentration trends of assays can sometimes be polynomial.

The application is programmed only to recognize one type of metabolite assay on one sensor, the instructions given to the user also explicitly mention that each sensor corresponded to one specific test; this helped to eliminate situations where two assay tests result in the same color but have drastically different metabolite concentrations. When a sensor reading is taken, the application will receive the measurement through BLE and check which sensor the reading was taken on. After the code has determined the sensor number, it will apply the sensor-to-sensor calibration and calculate the color number given the equation that is associated with the sensor, and this color number will then be matched to the assay calibration curve that corresponds to the sensor used. Lastly, the app obtains the back-calculated metabolite concentration and saves it into the measurement result SQLite database.

In the previous version of this application, the raw assay calibrations curves values were saved to a raw values SQLite database, and the application had queries to access this database. It used linear and quadratic regression functions to calculate the color weight and apply it to every measurement. However, as more testing was conducted, the color weight values were deemed adequate. Thus, a single equation is saved instead of the raw calibration curve. This change decreased the package size of the application and freed up computational power during measurements.

Chapter 4

Testing Sensing Platform

Two versions of sensor devices were developed: the 96-well plate sensor platform device and the 3-well sensor platform device. The two devices were designed to suit different needs but operate under the same principle. Since the 3-well sensor device had a newer and easier-to-use design, most of the testing was done on the improved build. Testing on the 96-well sensor device was mostly done for troubleshooting purposes. The results obtained on the 96-well sensor device held no significance, but they offered vital insights into some software and hardware bugs. Testing on the 3-well device was done using colored water solution, colored resin block, and colorimetric reactions. The tests gave valuable information regarding precision, accuracy, sensitivity, stability, and other device performance statistics.

4.1 Colored water test

In order to assess the performance of the TCS34725 color sensors, it was necessary to determine the accuracy and precision of the sensors. However, testing using pooled urine and actual enzymes during the debugging phase can become expensive, so as a cost-effective solution to test the sensors, food coloring mixed in water is used to produce a measurable sample that mimics the color of the metabolite assays.

4.1.1 Sensor precision test

The precision of the sensor was tested by measuring the same colored water sample multiple times and comparing the results to determine if variations between each measurement were observed.
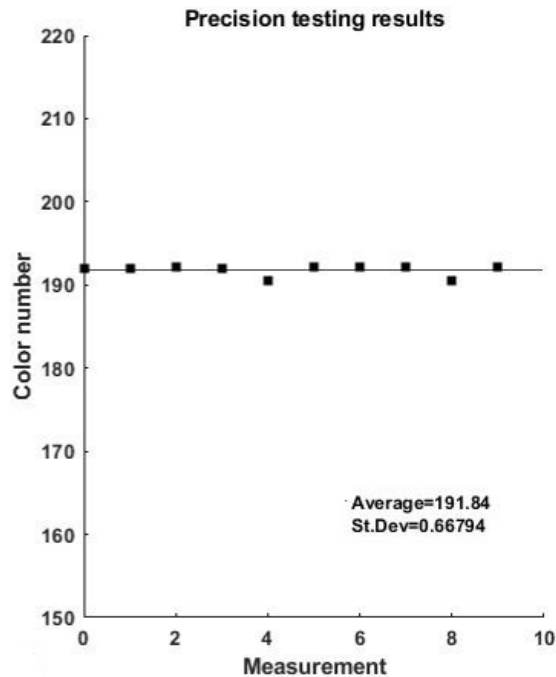
Figure 4.1. Raw red value plots for ten measurements tested using the same sensor on the same sample.

The graph in figure 4.1 compares the raw red color values obtained from the sensors throughout the ten measurements since the water sample was predominantly red. There is minimal variation observed between the ten data points from the graph, as seen from the 0.48 standard deviation value, hence stating that the sensor is precise.

4.1.2 Sensor accuracy test

The accuracy of the sensor device was determined by measuring colored water samples of increasing concentration. First, the colored water stock solution was prepared as follows: 6 drops of red dye and 3 drops of yellow dye were mixed in 250 mL of water. Then 10mL of this stock solution was labeled as the 100% sample. Next, 9mL of the stock solution was mixed with 1mL of water and labeled as the 90% sample. The dilution was repeated until ten samples were created from 10% to 100%. The ten samples created were put into fluidic cartridges and measured on the same sensor to obtain a calibration curve. This was then repeated three times to obtain the error bars. As can be seen in figure 4.2, the trend is linear with a coefficient of determination of 0.99.
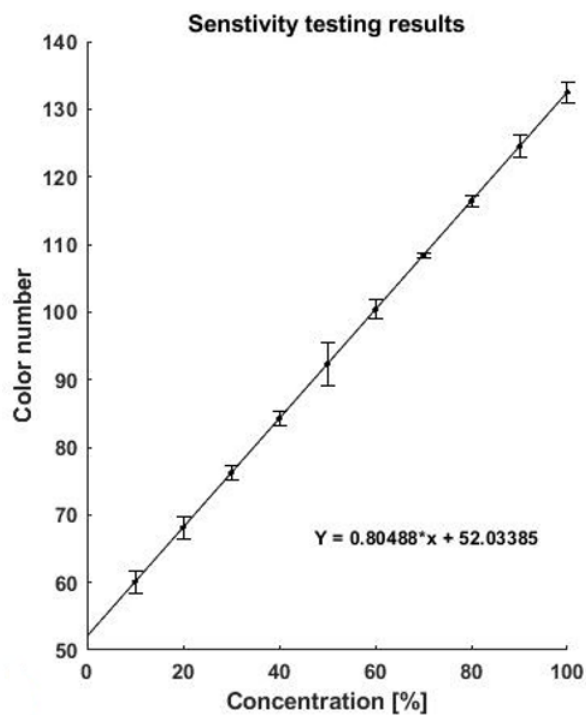

Figure 4.2. A plot of the Red value curve for the ten samples measured using the same sensor.

4.1.3 Sensor sensitivity range test

The sensor platform is designed to work with colorimetric metabolite assays of all color ranges as long as the color intensity scales with concentration. Therefore the working color range of the color sensor has to be tested for a wide spectrum of colored samples.
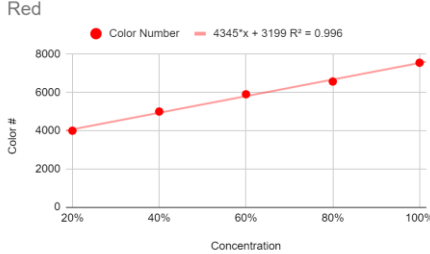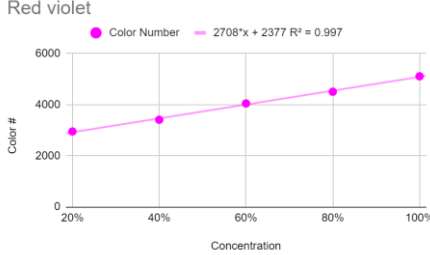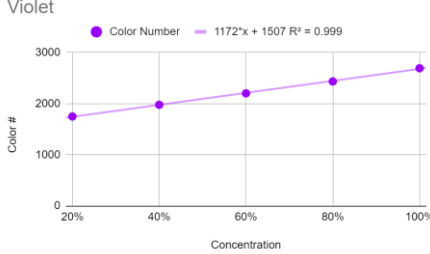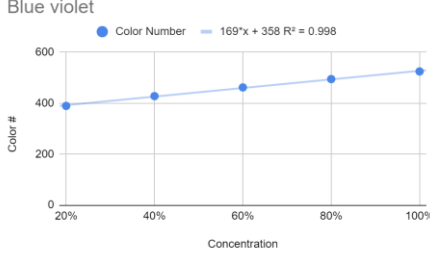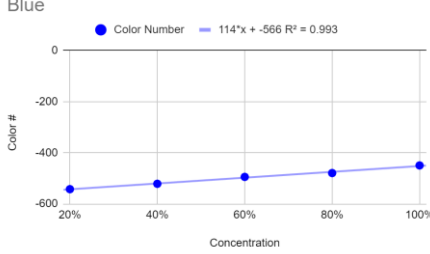

Figure 4.3. Twelve colored fading spectrum created using food coloring and water.

Shown in figure 4.3 is a batch of colored samples that formed a twelve-colored color wheel of fading color intensity from 100% to 20% in decrements of 20%. I made three sets of colored water stock solution by adding 200 μL of food coloring into 60 mL of water. This is repeated for Red, Yellow, and Blue colored food coloring. Furthermore, a color wheel was made by combining two out of the three colored stock solutions in controlled amounts. 15 mL of yellow combined with 5 mL of red resulted in yellow-orange, 10 mL of yellow combined with 10 mL of red resulted in orange, and 5 mL of yellow combined with 15 mL of red resulted in red-orange. 15 mL of red plus 5 mL of blue resulted in red violet, 10 mL of red plus 10 mL of blue resulted in violet, and 5 mL of red plus 15 mL of blue resulted in blue-violet. 15 mL of blue added to 5 mL of yellow resulted in blue-green, 10 mL of blue added to 10 mL of yellow resulted in green, and 5 mL of blue added to 15 mL of yellow resulted in yellow-green. A total of 12 colored samples were created using the above method, then further diluted with water to 80%, 60%, 40%, and 20% of their original concentrations.

63

Since visible color measured on the sensor is filtered into their respective channels of red, green, and blue light, the colored samples measured are represented through the color number, which is a weighted combination of the values obtained on all three channels of the sensor.

Row Number	Color and composition	Calibration Curve from Sensor	RGB Weightings From Sensor
1	Yellow (100% yellow)	Yellow Color Number — 1022*x + 1252 R² = 0.984	R:5495.009777 G:150.7719961 B:-7695.084452
2	Yellow Orange (75% yellow, 25% red)	Yellow orange Color Number — 1546*x + 2288 R² = 0.991	R:9404.024877 G:-1067.816106 B:-7780.915051
3	Orange (50% yellow, 50% red)	Orange Color Number — 2240*x + 2828 R² = 0.998	R:12711.11128 G:-5819.233948 B:-6702.953623
4	Red Orange (25% yellow, 75% red)	Red orange Color Number — 2841*x + 2866 R² = 0.992	R:13663.18209 G:-8139.216042 B:-5349.540663

5	Red (100% red)		R:17201.82878 G:-11634.25898 B:-4691.176611
6	Red Violet (75% red, 25% blue)		R:13433.26131 G:-9913.328852 B:-3399.715716
7	Violet (50% red, 50% blue)		R:8713.434033 G:-7106.452008 B:-1388.931656
8	Blue Violet (25% red, 75% blue)		R:2726.285667 G:-3240.064841 B:3.79204882
9	Blue (100% blue)		R:-2732.470334 G:925.6664706 B:1726.36179
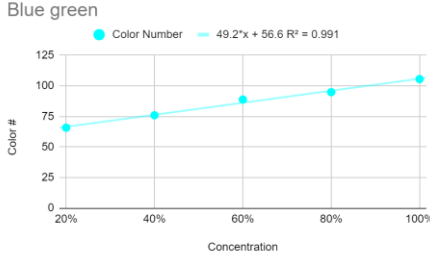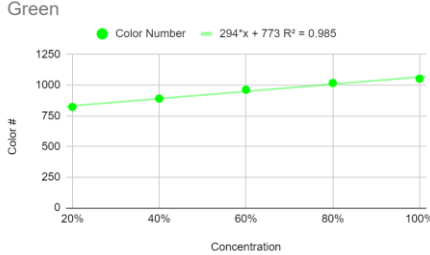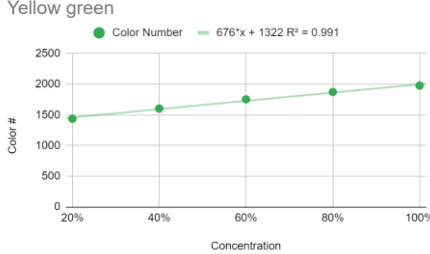
10	Blue Green (75% blue, 25% yellow)	Blue green — 49.2*x + 56.6 R² = 0.991	R:8.913484405 G:1163.121059 B:-1649.115248
11	Green (50% red, 50% yellow)	Green — 294*x + 773 R² = 0.985	R:2849.729069 G:1147.681453 B:-4095.840316
12	Yellow Green (25% red, 75% yellow)	Yellow green — 676*x + 1322 R² = 0.991	R:5074.724714 G:981.682694 B:-6253.859058

Table 4.1. List of all color spectrum samples curves and their respective weighting

The sensor was able to determine the linear change in the intensity of the color of the samples, as can be seen in Table 4.1. The trends observed in the color number showed were overall positive for all colors, which corresponds to the samples that were measured. Furthermore, even when the graphs all show an increasing trend, the RGB weighting for each sample varied depending on the composition of the measured light, which further indicated that the sensor is able to function with metabolite assays of many visible colors.

4.2 Resin test

Up until this point, all testing of the three-well sensor platform device was done using either colored water created from food coloring or using real colorimetric assays. Testing the colored water required preparation of the stock solution and further dilution to create a curve, the colored water cannot be stored since they lose its color intensity over time, and testing the metabolite assays requires collection and spiking of urine samples, consumption of materials (enzyme, dye, buffer, filters, etc.) and coordination with the chemistry team in most cases. I found both testing methods to be time-consuming and very unnecessary when it comes to quick testing of minor changes. The situation called for permanent testing solutions, and thus colored resin blocks were produced.

4.2.1 Resin block test

To replace the need for sample preparation every time minor changes were to be tested, resin blocks were made using epoxy resin from Magic resin, sold on Amazon, and epoxy resin dye from Let's resin, also sold on Amazon. A stock solution of yellow-colored resin was made and then diluted down to 90% of its original concentration, this process was repeated 10 times.
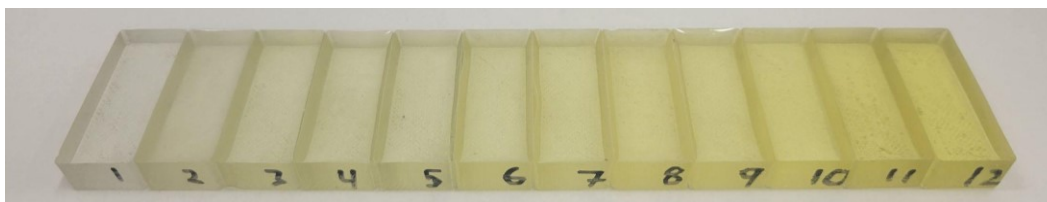
Figure 4.4. Yellow resin block set used for curve creation

The prepared resin mix was poured into an FDM 3D printed mold that is dimensioned according to the cartridges so they can fit into the cartridge tray. The resulting resin blocks are shown in figure 4.4.

However, problems were quickly noticed with this specific method of resin block preparation. First of all, the surface texture of the 3D printed mold was completely captured by the individual resin block once cured, this will affect the measurements, and we cannot ensure the next set of blocks will be the same as this. Secondly, the working time of resin is only 10 to 20 minutes, which means it's really hard to dilute the original sample as time goes on. Thirdly, resin often forms bubbles when mixed, and removing them requires the use of a vacuum chamber and the resin to be less viscous (figure 4.5), again, both of which come back down to the element of time.
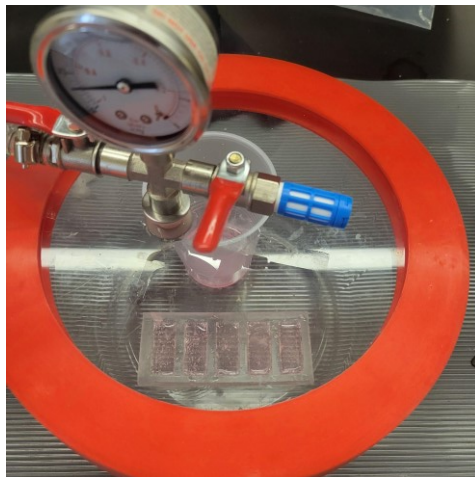
Figure 4.5. Using a vacuum chamber to eliminate bubbles in the resin blocks.

Lastly, the produced resin blocks have a much longer optical path length compared to the cartridges. Therefore it could not be used as a close comparison to the samples within a cartridge.

4.2.2 Improved Resin block test

Learning from previous mistakes, changes were made in the manufacturing process of the new resin block. The first change that was made was to the mold, instead of FDM 3D printing which can show layer imperfections, SLA 3D printing was used to produce the reverse mold needed to create the PDMS mold. Using a Formlabs 3b+ resin printer, the reverse mold was printed and polished to remove any surface imperfections. Next, PDMS was mixed and poured into the resin-printed reverse mold, and this was then put into the vacuum chamber and then finally heated at 100 degrees Celsius for 1 hour to harden. Note that polishing of the reverse mold has to be done thoroughly in order to achieve a smooth finish in the final resin block. Another way to get around this issue is by coating the inside of the PDMS mold that comes into contact with the resin reverse mold with a thin layer of PDMS after demolding it. This method will utilize atmospheric pressure to help create a smooth surface on the inner faces.

To address the second issues that were encountered in the previous attempt, precise amounts of clear epoxy resin and resin dye were defined for each resin block, this process allowed me to make one set of 5 resin block without worrying about the working time of the resin and will result in a set of resin blocks of the same color that can be used for calibration purposes. The resin block and molds are shown in figure 4.6 down below, the resin blocks are created using 20 g of resin together with 17 g of hardener. Two batches of the resin block were created as prototypes, one had 400 uL of dye, and the other had 200 uL of dye.
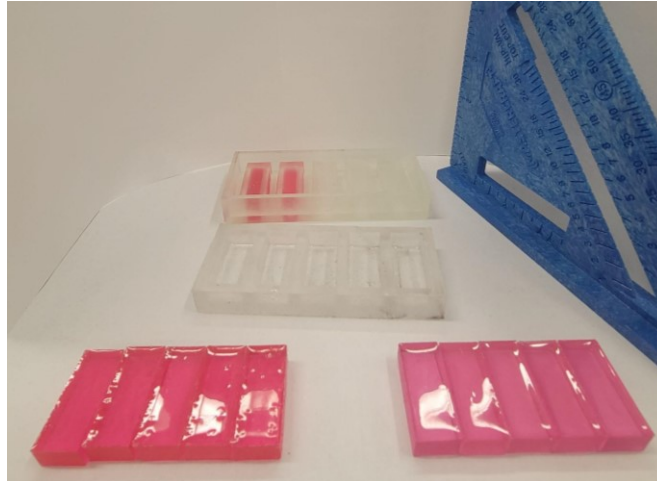
Figure 4.6. Version 1 of mold and resulting resin blocks

Lastly, as shown in figure 4.7, the shape of the mold was adjusted so the final produced resin blocks are 6mm in height, which would closely resemble the cartridges. Each batch of resin blocks are created using 10 g of resin and 8.5 g of Hardener, the first batch of blocks contains 50 uL of dye, while the second, third, and fourth batch of the resin contained 100 uL, 150 uL, and 200 uL of dye, respectively.
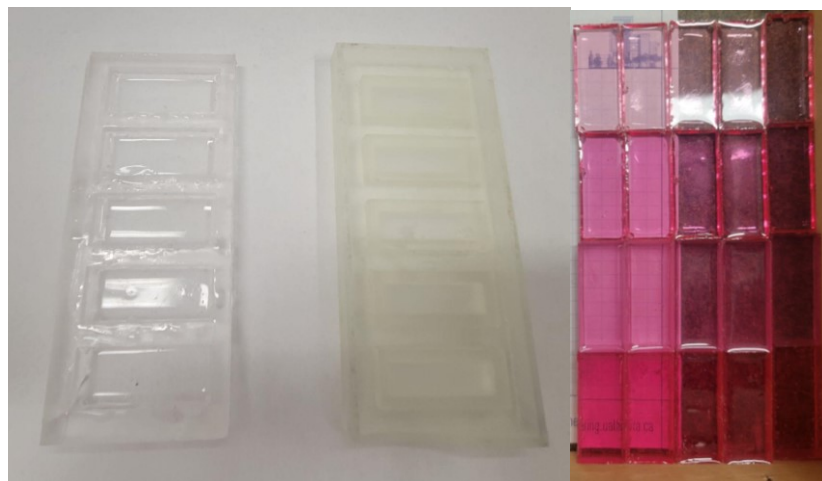
Figure 4.7. Version 2 of the molds and resin blocks

4.2.3 Sensor to sensor calibration

Amongst the three available color sensors within a single sensor platform device, each sensor could have a slightly different reading even when measuring the same sample. This issue exists because, firstly, the sensor is highly sensitive, and the slightest change in lighting can bring about significant changes in the result, and secondly, there exist inherent differences in the sensor units themselves, hence why sensor-to-sensor calibration is needed to ensure comparable results are measured from all sensors for the same test or sample regardless of differences between sensor devices.

One specific sensor unit was set aside and used as the standard, and this was sensor 0 on the reference sensor device. The reason behind it was that sensor 0 was the first sensor on the first prototype device made, and the majority of the tests and data collection were done using that specific sensor. So now, all other sensors are first calibrated to the reference sensor device's sensor 0 before being used to collect data.

The process by which we ensure identical sensor measurements are obtained is as follows. Measuring the same set of samples with increasing color intensity on two different sensors will provide two sets of ARGB data, we can break up the data into individual colors and plot the color data using a linear approximation for every color. From here, we matched the equation of the line for one sensor to the line equation of the other sensor by scaling the slope and matching the intercept and noted what the scaling factor and what the shift in the intercept is. When a measurement is taken on the non-reference sensor, we can subject the data to the scaling and shift factor for every color, and then this data would represent what the measured value should have been if it was measured on the reference sensor.

Calibration of the sensor was conducted using ten samples of the prepared colored water solution, similar to the previous test, and all ten samples were measured on the first sensor and then also measured again on the other two sensors.
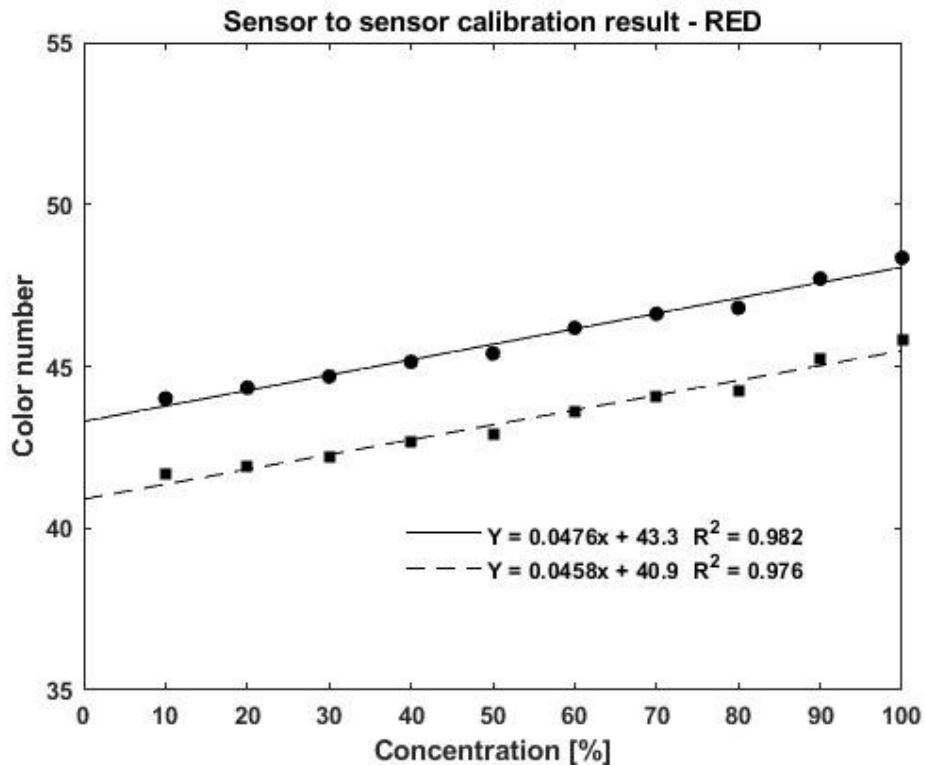
Figure 4.8. Plot of sensor-to-sensor calibration results for the red data

Figure 4.8 shows the difference between the percent red color data values captured for Sensor 0 and Sensor 3. By shifting the linear function of Sensor 3 to match the Sensor 0 y-intercept, and then scaling the curve such that the two slopes match, Sensor 3's percent red data values were calibrated to match Sensor 0 percent red data values. This process was repeated for each photodiode and for each color data - red, green, and blue. Any future measurements done using Sensor 3 will be subjected to this y-axis shift and scaling factor. Thus, the outcome will be the same as that of Sensor 0. In the final programmed application, this data processing operation is automatically done, and the user will not need to manually calculate anything.

4.3 Assay test

Testing with colorimetric assays was conducted after colored water and resin testing was complete. Commercial pooled urine purchased from Lee Biosolutions (Maryland Heights, USA) was spiked with known concentrations of a chosen metabolite and then assayed to produce the colorimetric sample that is to be measured on the sensor platform.

4.3.1 Creatinine test

One of the metabolite biomarkers chosen was creatinine. This metabolite is a byproduct of muscle protein metabolism. Since it is produced and then removed at a constant rate, it can often be used to normalize urinary metabolite concentrations to account for varying levels of hydration. As mentioned before, the usage of the Jaffe reaction contributed to the production of a colorimetric assay that can be used to determine the concentration of creatinine in urine[47].

To test the sensor performance on real colorimetric assays, a stock solution of creatinine was first prepared in water to a final concentration of 120 mM. Ten calibration curve standards containing 3.8, 6.7, 9.6, 15.4, 21.2, 27, 32.85, 38.6, 44.4, and 50.3 mM creatinine were prepared by mixing 0, 25, 50, 100, 150, 200, 250, 300, 350 and 400 μL of 120 mM creatinine stock solution in 1000, 975, 950, 900, 850, 800, 750, 700, 650 and 600 μL of PU, respectively. The proposed process will create 10 samples of spiked and diluted creatinine samples that can be used to create a calibration curve. Also, the created

73

curves will be tested on both the lab owned spectrophotometer (Biotek Synergy HT) as well as our developed sensor platform device.
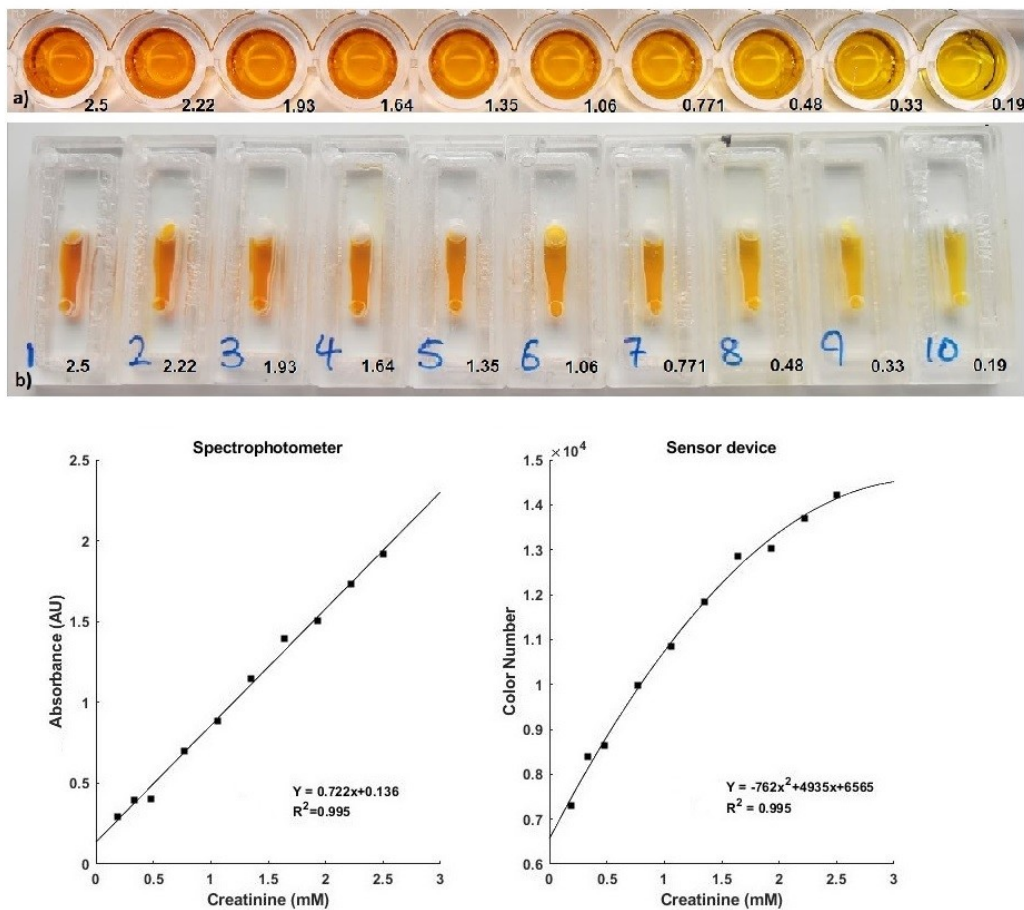
Figure 4.9. Ten samples of urine spiked with Creatinine, diluted 1/20, and then assayed using the Jaffe assay. The resulting sample is loaded into a) 96-well plates to be tested in a spectrophotometer and b) cartridges. Actual(diluted): 50.28 (2.5), 44.47 (2.22), 38.66 (1.93), 32.85 (1.64), 27.04 (1.35), 21.23 (1.06), 15.42 (0.771), 9.61 (0.48), 6.71 (0.33), 3.80 (0.19) mM. After 10 minutes of incubation, the absorbance of the creatinine-picrate complexes was measured at 490 nm in the spectrophotometer, and the quantitative color was also determined using the sensor.

From figure 4.9 shown above, the spectrophotometer data and the sensor data were plotted side by side for comparison, and we can notice that the spectrophotometer

data demonstrated a linear trend, whereas the data that was obtained from our developed sensor device showed a polynomial trend. Also, for the sensor data, the initial data was linear, but the linearity began to disappear at 1.25 mM creatinine.

This is likely due to the calculation method and fundamental concept of the developed sensor platform device. The spectrophotometer measures light at a specific wavelength but our developed sensor will measure light in the visible light spectrum. From the plot of spectrophotometer data, the observed linear trend means the absorbance of the sample does increase linearly at the target wavelength. If we expand on the observation, we can assume that the proportion of received light at other wavelengths will decrease as the concentration of the metabolite in the sample increases. Knowing the weighting for each color is determined by the change in the percentage of received light at that wavelength. If the trend is less predominant, the weighting will be less, and vice versa. Also, note that the weight coefficient is often in the scales of 10^3 to 10^4 range. Therefore, the effect of the received light in the nondominant wavelength region of the spectrum decreases as the concentration of the metabolite increases, hence the nonlinear trend is observed on the sensor platform device output.

To assess the accuracy of the created calibration curve, a few quality control samples were tested, and the concentration was calculated using the curve, and the results are shown in figure 4.10.
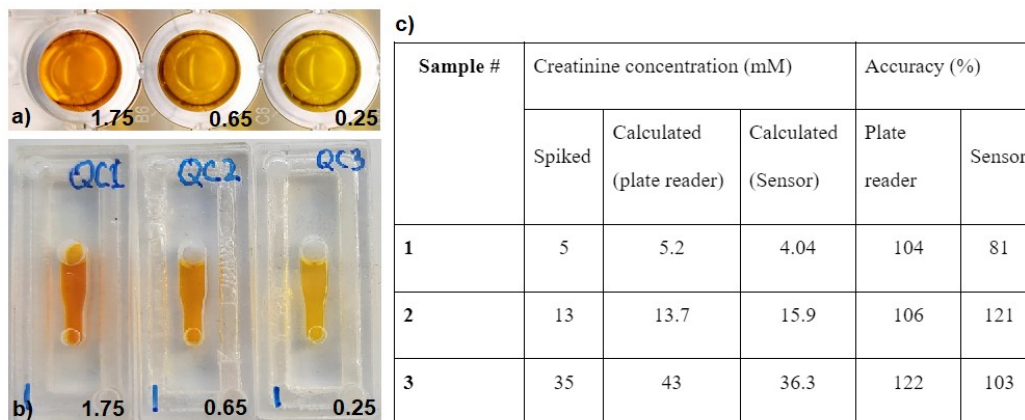
Figure 4.10. A comparison of the sensor to spectrophotometer measurements High, medium, and low concentrations of creatinine were measured in a) 96 well plates using a spectrophotometer and b) the fluidics cartridge using the sensor. c) Table comparing the accuracy of results. Actual(diluted): 35 (1.75), 13 (0.65), 5 (0.25) mM.

From figure 4.10c) We can see that the accuracy of measurements taken on the sensor platform device was better(103%) when the creatinine concentrations were higher (above 20 mM) while yielding a lower accuracy at the lowest concentration (5 mM) but were still within the acceptable range of results (±25%). Overall the results are comparable to results from the spectrophotometer.

4.3.2 New Creatinine test

The picric acid used in creatinine assay steps causes problems with shipping and storage because dried picric acid is explosive when exposed to heat or shock. Although the amount of picric acid used per test is minuscule, international shipping companies will still flag it due to its explosive nature. Therefore, the chemists here at the Wishart laboratory have opted to develop a new assay to determine the concentration of creatinine in the urine sample.

With the new reaction, the formulated color in the colorimetric assays is different, and thus the calibration curve needed to be recreated to account for the change in color formation. Ideally, the calibration curve should have a low Limit of Detection(LOD) as well as a low Limit of Quantification (LOQ), this makes the curve accurately recognize a large range of data points and be able to distinguish between similar data points. Results for the new calibration curves are demonstrated in figure 4.11, the range of detection on this calibration curve is between 3.6 mM to 51.8 mM.
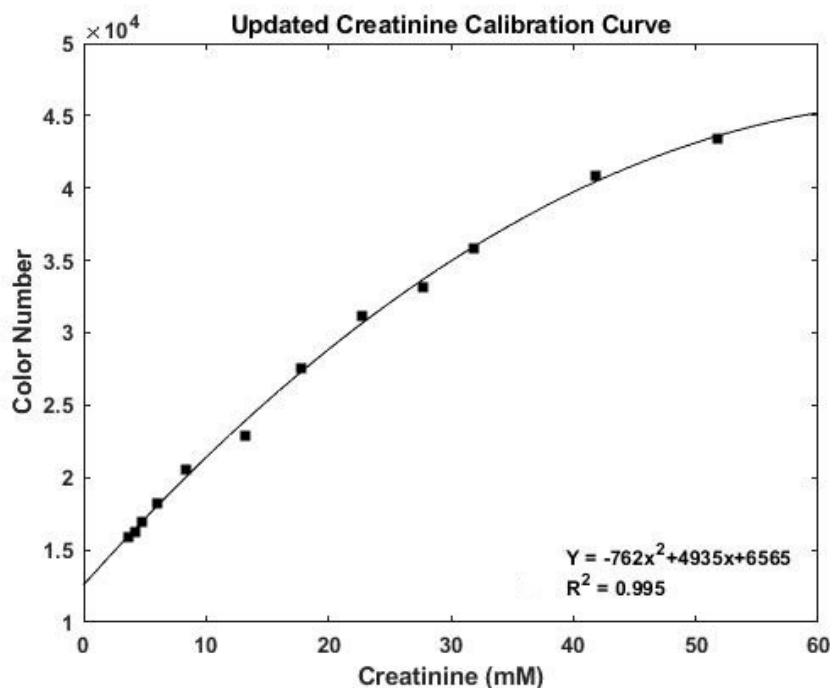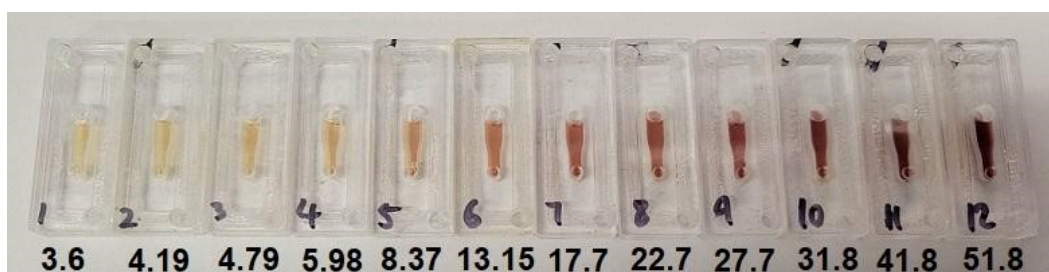
Figure 4.11. Twelve samples of urine spiked with Creatinine are loaded into individual cartridges, quantitative color was determined using the sensor and plotted.

Chapter 5

Workstation design

The colorimetric assays developed in the laboratory can sometimes be complicated and require trained personnel to carry out. On top of this, the assays sometimes deal with enzymes and chemicals in amounts as low as tens of microliters. Therefore, even among skilled operators, differences in the output results can be measured when conducting the manual mixing, filtration, and processing steps due to the slight differences when carrying out the procedures. Furthermore, human errors are a source of random errors, which are detrimental to any scientific experiment. Therefore, by automating the assay preparation steps as much as possible, we aim to eliminate random errors and keep all future errors systematic and easily resolvable. Since the project aims to design an accessible sensor platform, the automation of assay procedures can help lower the requirement to become a skilled operator.

The workstation was designed to assist in the coulometric assay preparatory steps and is to be used in conjunction with the sensor device that carries out the final measurement step. For the sake of user control simplicity, the workstation can not function on its own. However, it will instead offer a wired mounting slot for the sensor device, in which the workstation controller chip can connect to the sensor device. All the workstation activities are first initiated by a signal from the sensor device and then driven by the preprogrammed workstation controller chip.
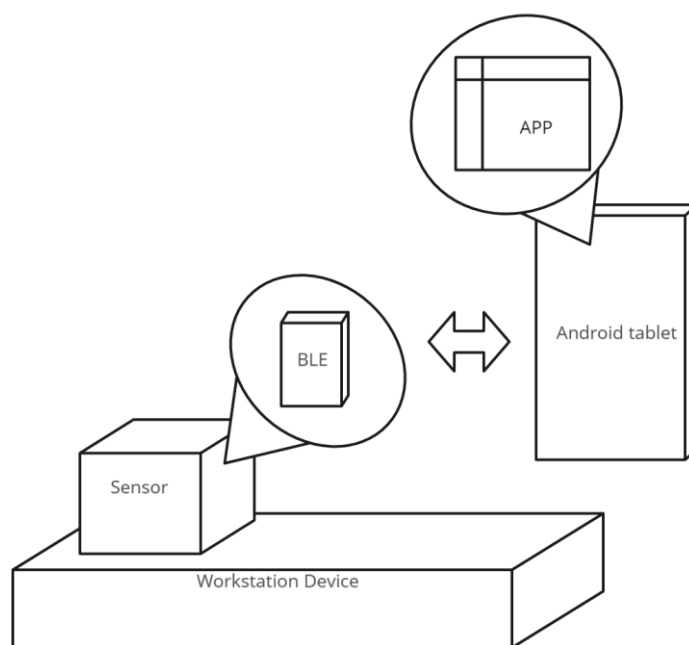
Figure 5.1. Conceptual diagram of the control scheme for the workstation device

As shown in figure 5.1, the Bluetooth-connected Android device will control what signal is sent and what procedures are carried out. This control scheme helped combine two separate devices into one complete system with an agent device driven by the master. For identification purposes, any mentionings of the sensor device in this chapter will refer to the standalone black box device that houses the physical color sensors. The term workstation will then refer to the platform that holds all the individual microfluidic systems that make up the complete process.

Together with all members of Tricca, we aim to bring this device from concept to reality. My work is mainly towards the electrical and programming aspect, together with the post-assembly phase beta testing and troubleshooting. Please note that the workstation is still under testing during the preparation phase of this manuscript, and therefore this chapter will not include any data collected from the device.

5.1 Dilution setup

Dilution is an essential process in the preparation of colorimetric assays. By controlling the dilution ratio of the base entity, whether it is urine or serum, we can manipulate the color output of the assay such that the concentration of the desired metabolite falls within a measurable range. The colorimetric assays that our workstation is designed to work around require dilution ratios of 1:10 and 1:30. By using two peristaltic pumps, we were able to move a controlled amount of liquid from two separate fluid reservoirs into a single output container, thus achieving the desired dilutions. The difficulty in this process lies in achieving the desired accuracy in the peristaltic pump when moving fluids. Therefore, to fully understand the issue, some background information regarding how peristaltic pumps function is required.
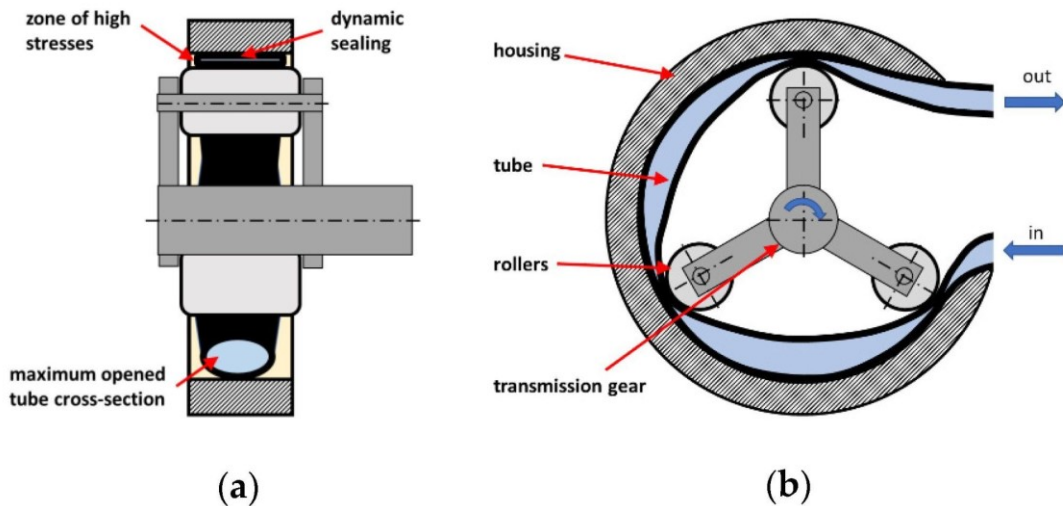
Figure 5.2. Flexible tube based peristaltic pump principle with 3 rollers; (a) cross-section of the pump in frontal-view; (b) cross-section of the pump in side-view.[55]

Shown in figure 5.2 is the conceptual design for a generic peristaltic pump. Peristaltic pumps operate using negative pressure created by rolling rollers across a section of deformable tubing, and this action creates a vacuum within the tube that pulls content in through the inlet while the contents already within the tube get squeezed out from the outlet. The concept can be thought of as squeezing out an infinitely long tube of toothpaste. A peristaltic pump can have any number of rollers attached to the center rotor, and they can be spaced out in any pattern at a 360-degree angle. The rollers will make contact with the tubing and exert the necessary force to pinch it close, thus creating a vacuum point, and the arc distance between one vacuum point to the next will determine the pillow size. As the motor turns the rotor, this pillow created by the two vacuum points will travel through the tube carrying its content from the inlet to the direction of the outlet. Thus, to design a successful dilution system, it is necessary to collect some data regarding the volume of liquid that a single pillow can carry, the precision of each pillow, the number of steps required to transport one pillow using a stepper motor as the driving source for the rotor, and the accuracy of the final resulting output volume.

Testing conditions are listed as follows: A NEMA 17 stepper motor rated at 12V and 1A, purchased from Digi-Key Electronics, is used. This motor allows for 800 steps per revolution, and there are six rollers positioned 60 degrees apart around the rotor shaft. The tubing purchased from McMaster-Carr is the High-Temperature Soft Rubber Tubing for Air and Water with a 4mm outer diameter and 2mm inner diameter. The pump was also allowed to run initially to prime the line using water. The tested peristaltic pump is shown in figure 5.3.
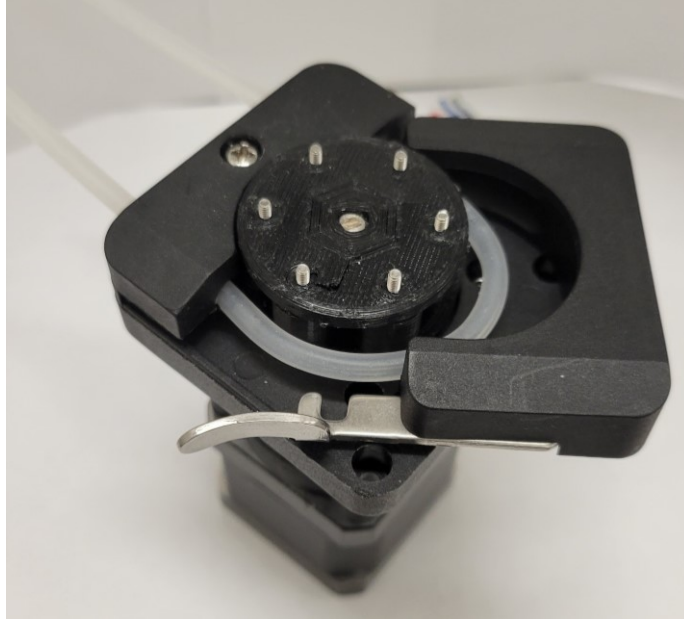
Figure 5.3. Peristaltic pump made using a stepper motor and gearbox, paired with flexible tubing.

The testing process can be outlined in 4 steps. First, the inlet tubing was connected to a reservoir of water. Secondly, a scale was set up with a container laid on top of it to collect water from the outlet. Thirdly, the stepper motor powering the peristaltic pump is coded with a program that lets it operate at 1 step per second. Lastly, the pump was set to operate continuously while data was being collected regarding the output volume of the water (assume a closed system and the density of water is 1 g/cm^3).

The collected results show that each pillow created by two vacuum points carries 33.69 microliters of fluid on average. This information was taken into account when programming the dilution process. Knowing each full rotation of the rotor is 800 steps for the stepper motor, each roller is 60 degrees apart, so 133 steps roughly separate one vacuum point from the next. Note that this data will only apply to the specific setup used for testing, and any changes to the tubing will drastically alter the output result.

5.1.1 Linear rail system

Due to the need for different dilution processes between each assay, the output of the dilution setup must go towards separate collection tubes based on the dilution that is being conducted. After some group discussions, the proposed solution will move the position of the collection tubes rather than the output end of the peristaltic pump tubing, such that we can avoid the potential effect of pulling on the peristaltic pump tubing.

The first design utilizes a linear rail system powered by a stepper motor to move a tray of collection tubes horizontally under the output nozzle of the peristaltic pump. This system consists of two support rails on the side and an M6 thread steel rod with a pitch of 1 mm acting as the center rail. All three rails are laid horizontally, and a 3D printed platform with bearings attached on the bottom is mounted across the three rails such that it can smoothly move left or right depending on the direction in which the center rail is spinning. In addition, since the stepper motor's rotor is directly connected to the threaded rod, the spin ratio is exactly 1:1, meaning one full rotation on the stepper motor will also cause the threaded rod to spin, thus moving the mounted platform 1mm to either direction, this direction will depend on the direction of the motor and the orientation of the threading on the rod. On top of the platform are falcon tube holders, which can hold the 15 mL falcon tubes used for collecting the outputs of dilution. Furthermore, the end of the output tubing from the peristaltic pump is connected to a nozzle located directly above the line of motion of the collection tubes.
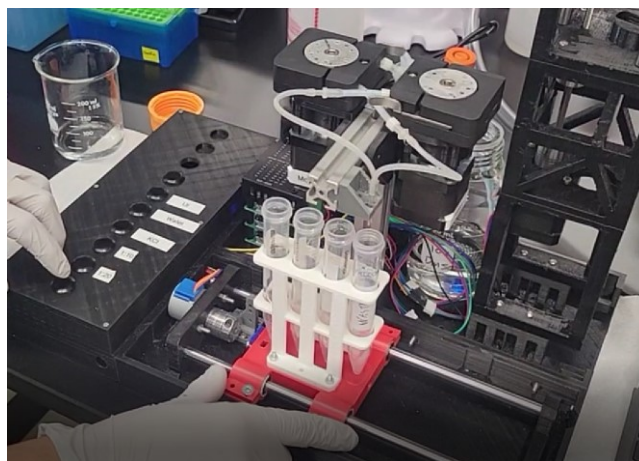
Figure 5.4. Testing of the linear rail dilution system.

Figure 5.4 shows the designed linear rail system, this design was tested and proven successful, but the large amount of space this setup uses caused us to work towards redesigning this system.

5.1.2 Rotating turntable system

Since the initial design had to be changed to reduce the total footprint of the device, the new design introduced a turntable system, which now uses one stepper motor to turn a sizable 3D-printed rotor piece. The rotor piece is equipped with mounting points for falcon tubes on its outer perimeter, and the output nozzle of the two peristaltic pumps is stationed at one point on the edge of the rotor. The turntable would rotate between dilutions to direct the outputs to their respective collection tube. There are eight mounting slots placed 45 degrees apart around this turntable for 15 mL falcon tubes for a total of eight possible dilutions. Only four are currently set up for this project, with one slot for waste collections and three more for dilutions. This new design, shown in figure 5.5, cuts down 65% of the required space, and the stepper motor action is reduced since it only needs to spin for one rotation for all the dilutions.
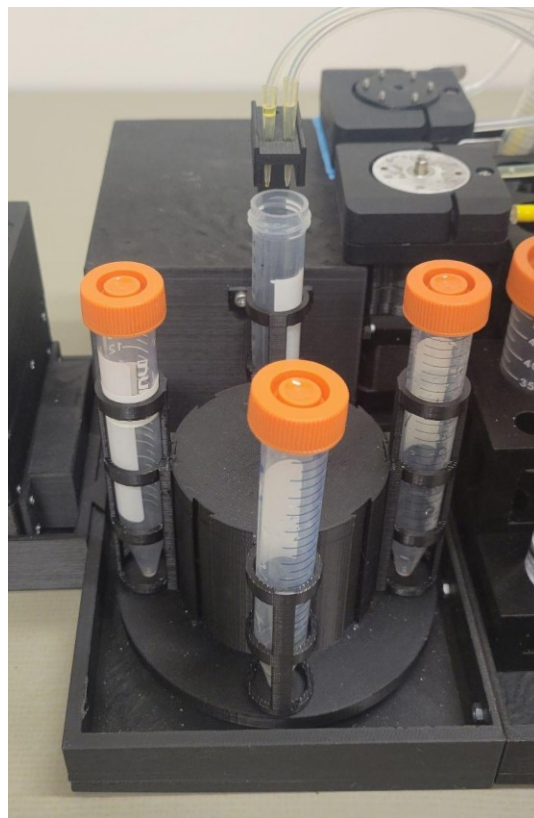
Figure 5.5. Testing of the rotating table dilution system.

5.2 Filtration setup

One key aspect of any fluidic system is the method of fluid transportation, and the peristaltic pump mentioned earlier was one of them, but additionally, there exist options like pressure-driven pumps and syringe pumps. However, pressure-driven systems used in microfluidics are harder to design, and existing market products are often more expensive[56]. Whereas, Syringe pumps, on the other hand, are a cheaper alternative and can be modified easily to suit the needs of this project.

The filtration setup is primarily designed for the diacetylspermine assay, but other assays will also use part of the setup. As the name suggests, the filtration setup filters out unwanted components from the urine sample while trapping the desired metabolite, the

main component of the assay process is the resin filters made by the chemistry team. The filters mentioned are not to be confused with typical syringe filter attachments, these filters are made by packing small resin beads tightly into the barrel of the syringe.

The filtration process is a two-part process where the first part requires liquid to move through one large resin filter; from here, additives must be introduced to the second small resin filter before more liquid can be passed through. The second part of the process requires the next fluid's flow rate from the second small resin filter to be controlled.
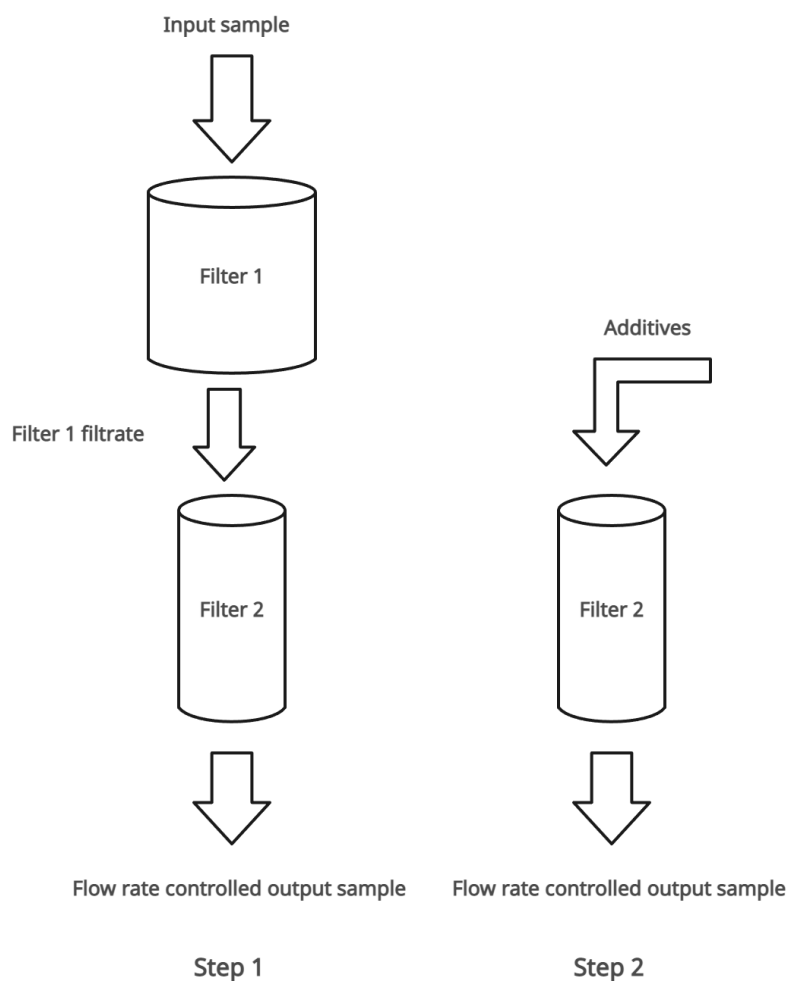
Figure 5.6. Conceptual figure of the filtration process with steps 1 and 2.

Shown in figure 5.6 is the conceptual figure for the two-part process. The difficulty level of this situation is escalated simply due to that one extra step where the additives have to be mixed. Since the additive cannot be passed through the first resin filter due to potential contamination, the connection between the first and second resin filters can not be closed. Also, as a bonus, both resin filters exist as a part of a syringe, meaning if they are attached to a syringe pump, both can be used to move liquid.

5.2.1 Negative pressure filtration

Given the requirements, fellow members of my lab settled on building a negative pressure setup[57] where the liquid is pulled through the system using a syringe pump. The first syringe is orientated upright with the plunger pulled out and opened to the atmosphere. The output of the first syringe is securely connected to the opening on the second syringe using an air-tight connector piece. With both syringes stacked vertically, the output of the second syringe is now attached to a connecting falcon tube lid piece, and another inlet is cut out from the lids for the negative pressure syringe pump connection. When the lid is screwed onto a falcon tube, a vacuum is created at the output, liquid in the first syringe is then pulled through and out of the second syringe. With the help of gravity, the filtered liquid will fall to the bottom of the collection falcon tube. This process is modified and repeated for the different types of liquid that need to be filtered. For example, some additives only need to be passed through the second resin filter, so the first syringe is removed from the top, and liquid is added to the second syringe instead.

The main focus of this system is to produce a controllable and consistent flow rate throughout the assay process, which can solve issues introduced by manual filtration. As mentioned before, most human errors come from inconsistent flow rate control and varying final volume, and the filtration setup aims to eliminate these errors.

The first model built by my fellow labmates was a proof of concept to see if the design would work as intended and if liquids could pass through the system and be collected at the bottom falcon tube. However, after some testing, air leaks appeared between the connection, and the flow rate became hard to control. The second issue was thought to be related to the first issue, and we could achieve better flow rate control if we

had a more secure connection in the lid. However, after further testing, it became evident that a consistent flow rate would not be achievable with this setup. In addition, looking back at the design of the vacuum system, the strength of the vacuum created by a syringe pump would decrease as the liquid is pulled through the system since the achievable pressure is limited by the distance at which the plunger can pull back. One possible solution for this issue could be to use an extra large syringe pump as the vacuum source, which would cause the change in vacuum strength to be insignificant for the amount of liquid in this experiment. Another solution would be to use a motorized air vacuum pump, but time limitations with the project prevented us from placing orders for larger volumed syringes or air pumps.

5.2.2 Positive pressure filtration

Me and a fellow member of the lab later developed a method to achieve a constant flow rate during filtration through the use of positive pressure setups. When applied to the situation here, the syringes holding the resin filters would act as the syringe pumps, and the syringe plungers would push the liquid out of the chamber through the filters when force is applied. The setup would be similar to the negative pressure setup, the two syringes would connect using a connector piece, but instead of being open to the atmosphere, the top syringe is first filled, then a plunger is attached to the back and inserted into a linear rail system. The output of the second syringe, depending on the type of input fluid, is now openly connected to different tubes for later use in different situations. Additionally, depending on the type of liquid to be filtered, one could remove

the top syringe and replace the plunger such that liquid added to the second syringe can now be pushed through. The benefit of this design is the improved flow rate control.
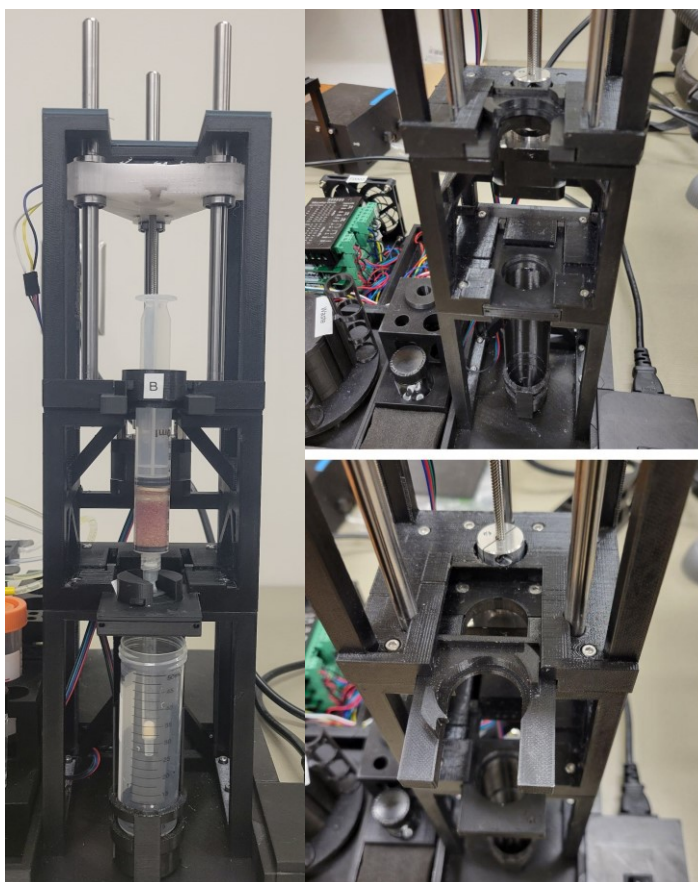
Figure 5.7. Workstation filtration system

Shown in figure 5.7 is the designed filtration tower with a close-up of the syringe mounting slot. In essence, this device has now become a replication of how a human would carry out the manual filtration procedure, but the advantage is that the machine can limit the possibility of error, and flow rate consistency could be achieved with every experiment. The proof of concept model of the device was built from salvaged parts from the dilution linear rails system. The results were auspicious, and we were able to obtain a flow rate as low as 30 microliters per 10 seconds from the second syringe filter. However, using positive pressure as the source for fluid movement means this whole process could

not function without user intervention after each step, and since the liquid is now added into the syringe and then placed in the linear rail, the user would have to go through more steps to fill the syringe and place the plunger. Therefore, the whole process is broken up into smaller steps, and each step has its associated sequence of motor movements, which will be coded onto the motor controller and then controlled by the user.

Figure 5.8. Complete workstation device.

5.3 Motor Controller

The processor used for controlling the workstation is an ATMega328P-U microprocessor, but this chip is also connected and controlled by the MCU PCB in the sensor device, acting as the agent peripheral for the master sensor device. The workstation has four stepper motors, one limit switch, and one magnetic switch that works together

91

to operate every procedure assigned to the workstation. Figure 5.9 shows the breadboarded controller circuit in the prototype device.
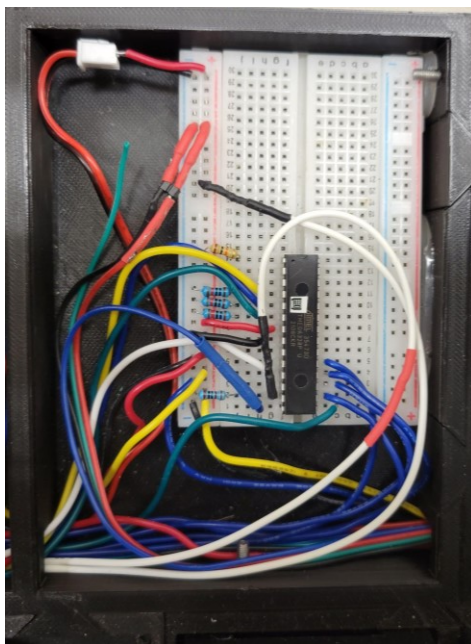
Figure 5.9. Workstation controller circuit.

Two of the four stepper motors are used to operate the peristaltic pumps in the dilution setup, and these would only require two output pins on the microcontroller since they would only need to be on or off. Note that stepper motors are paired with TB6600 4A 9-42V stepper motor drivers (purchased from Amazon). These drives only require two connections to operate, one for steps and the other for direction, which controls the direction of spin for the rotors to be either clockwise or counterclockwise for high or low input, respectively. The two peristaltic pumps will only move liquid in one direction; hence the direction pin will be permanently set to low. The speed of the motor is determined by the delay between pulses sent to the step pin, and operation time is simply determined by the total duration of the pulsating signal sent to the step pin.

Additionally, the turntable dilution setup has a single-direction spin for its operating stepper motor since the falcon tubes around the turn table can be reset to their

original location after one full motor rotation with no reverse moments required. As an added insurance, the turn table also has a small 5 mm round magnet mounted on the side that would operate together will a magnetic switch that would be pulled open when the round magnet is within a 3mm proximity, and this switch is mounted on the side of the case that houses the turntable, hence, setting this position to be the starting position. The turntable system also requires two pins, one for the power input of the motor and one for monitoring the state of the magnetic switch.

The last of the four stepper motors in the workstation is paired with the limit switch, which is used to operate the linear rail systems in the filtration setup. This stepper motor will spin the threaded rod to move the connected plunger holder platform up and down in a vertical direction. Hence the motor controller microprocessor will require an additional output pin for controlling the direction pin of the stepper motor. Next, when the platform reaches the top of the rail, it will hit the limit switch mounted on the ceiling to prevent it from spinning out of bounds and damaging the threads on the rod. This limit switch offers additional protection as well as feedback on the position of the plunger holder platform. Therefore, three pins are required on the motor controller chip to operate the filtration setup. Figure 5.10 shows the cascade of motor controllers and their placement on the workstation device.
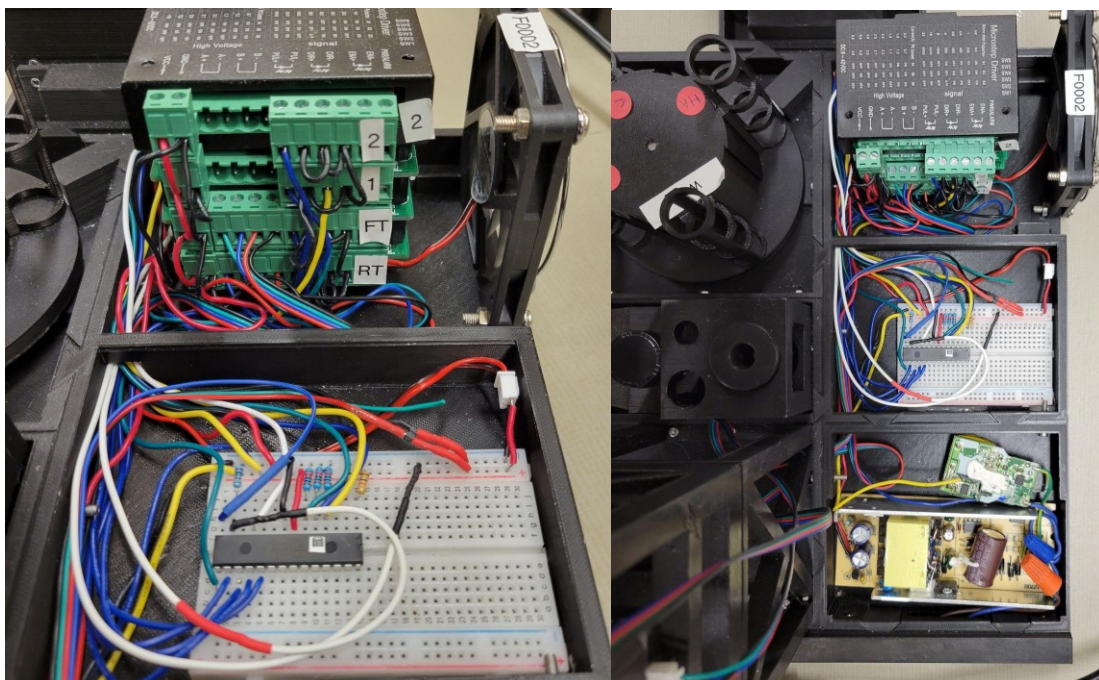
Figure 5.10. Workstation motor controllers and circuitry placement.

5.3.1 Motor input and output signals

Adding together all the required pins to the workstation device will result in seven output pins being occupied on the ATmega328P chip. A total of 28 pins exist for these ATmega328p chips, of which 20 can be used as input or output pins, while 14 out of the 20 I/O pins are digital, and the other 6 are analog. The seven pins required by the workstation only need to have high or low signal output, so any of the Atmega328p digital pins can be used.

The complete procedure to run the complete assay test is broken down into the following steps: reset workstation, dilution, urine filtration, first water filtration, second water filtration, salt water elusion, and then lastly, cleaning. Each of the above steps has its associated sequence of motor movement, and these sequences are coded into the microcontroller as a stand-alone function.

94

Using three pins as input signal pins, we can use a binary encoder function to encode eight functions, the seven steps mentioned above, and an additional idle state function, into the truth table of the three input signal pins. These signals will be sent from three select pins on the sensor device. The reason behind having a separate processor to control the motor is due to the need for multithread action on a single ATmega328P processor and the lack of additional pins to control the motors. Moreover, the measurement functionality of the sensor device depends on the internal timers of the Atmega328p in the sensor device, each sensor, and LED pair is assigned to a timer, and when the timer expires, the reading is taken. The whole process would be fine if the sensor device were to be used independently, but if the same processor were also used to control the motors, there would be pauses in the workstation procedure to allow for measurement of the samples when the timer expires, hence why another processor is used to manage the motor control functions. Additionally, an extra pin is used on both chips as a flag pin to report the working state of the agent to the master, eliminating the need for TX and RX pins for communication. The master device will read the state of the flag pin before setting the state of the select pins, and high reading means the agent device is idle and can be commanded, while a low reading indicates the agent is already processing a command, so the select pins are not set on the master device. The flag pin is inspired by the ACK signal within a data network. Finally, with this setup, we achieve an uninterrupted work process by simulating a dual-core system to allow for multi-threading functionality, which removes the use of timed interrupts, therefore, decreasing the difficulty in code writing. On top of that, more pins are available to use, so the workstation is available for future upgrades and expansion.

Chapter 6

Conclusion

First, a portable and affordable POC sensor device capable of quantitatively measuring color was built. The sensor was able to be controlled wirelessly through BLE, and measurement data could be stored and then sent back to the controller upon request. The sensor can be used to measure any colored sample 100 µL in volume using the lab-manufactured custom fluidics cartridge. Results from the testing showed that the sensor was precise, with a standard deviation of 0.46 when measuring ten samples of the same composition; also, the accuracy of the sensor is demonstrated by a coefficient of determination of 0.99 when measuring ten samples of increasing color concentration. The spectrum detection range for the sensor is extended to a twelve-colored spectrum, with each color showing a 0.99 coefficient of determination. When compared to a laboratory plate reader for distinguishing creatinine samples, the sensor device outperformed the plate reader when measuring high creatinine concentration samples, whereas the mid to low-range results performed slightly worse but still are comparable to the plate reader results.

Secondly, an Android application capable of controlling the sensor through BLE was created. On top of that, the application could receive measured data from the sensor device, process the received color data, achieve a diagnostic result for cancer, and save the data into a local database.

Lastly, an automation system was designed to assist the manual assay process such that the requirements on the operator to conduct screening tests can be lowered. The workstation device exists as a tabletop setup that BLE controls through the mounted

sensor device with the companion Android application. On the workstation, other than the mounted sensor device, there exists the dilution system and the filtration system, both of which are universally applicable to a wide range of chemistry applications.

In conclusion, the project initially required a POC device to screen for CRC cancer, we, the Tricca engineering team, were able to develop the biosensor suitable for that application successfully. Then by collaboration with the Wishart chemistry team, we were able to automate parts of the manual assay process, which increased the ease of use. Furthermore, we have created not just a specialized POC device targeted towards screening CRC cancer. Instead, we have delivered a general sensor platform device that can be used for most colorimetry applications. The project has grown past the initial expectation and is on its way to becoming a widely applicable and portable laboratory device.

However, this device is still limited by the chemistry aspect, it requires extensive studies to be done on the development of quantitative colorimetric assay before it can be used to identify biomarkers within a sample. In the near future, I aim to help develop a universally applicable full automation device that can be used in the assay process of different metabolites with minimal coding and physical modification required in order to measure a set of metabolites and achieve diagnostics. Currently, improvements are being made toward the full automation of the setup. We have moved on to using micro cuvettes to replace cartridges since they are more widely used in the field of spectroscopy and can eliminate the potential errors caused by the manufacturing process. Positive filtration has been replaced with a complex valve-based negative pressure setup that uses a custom peristaltic pump as its main driving force.

References

[1] M. L. C. Passos, M. L. M.F.S. Saraiva, "Detection in UV-visible spectrophotometry: Detectors, detection systems, and detection strategies," Measurement, Volume 135, 2019, Pages 896-904, ISSN 0263-2241, https://doi.org/10.1016/j.measurement.2018.12.045.

[2] J. H. Hardesty, B. Attili, "Spectrophotometry and the Beer-Lambert Law: An important analytical technique in chemistry." Collin Coll. Dep. Chem. (2010), 76−99.

[3] G. F. Lothian, "Beer's law and its use in analysis. A review," Analyst, 1963, 88, 678 DOI: 10.1039/AN9638800678

[4] D. Swinehart, "The Beer-Lambert Law" *Journal of chemical education* Edition 9, (1962), 333, 39(7)

[5] M. G. Mellon, "The role of spectrophotometry in colorimetry." *Industrial & Engineering Chemistry Analytical* Edition 9, no. 2 (1937): 51-56.

[6] B. Cunningham, P. Li, B. Lin, J. Pepper, "Colorimetric resonant reflection as a direct biochemical assay technique," Sensors and Actuators B: Chemical, Volume 81, Issues 2−3, 2002, Pages 316-328, ISSN 0925-4005, https://doi.org/10.1016/S0925-4005(01)00976-5.

[7] H. Wei , S. M. Hossein Abtahi, P. J. Vikesland, "Plasmonic colorimetric and SERS sensors for environmental analysis" Environ. Sci.: Nano, 2015, 2, 120-135, DOI: 10.1039/C4EN00211C (Tutorial Review)

[8] W. Zhao, M. A. Brook, Y. Li, "Design of Gold Nanoparticle-Based Colorimetric Biosensing Assays." ChemBioChem, (2008), 9: 2363-2371. https://doi.org/10.1002/cbic.200800282

[9] P. Baptista, E. Pereira, P. Eaton et al. "Gold nanoparticles for the development of clinical diagnosis methods." Anal. Bioanal. Chem. 391, 943−950 (2008). https://doi.org/10.1007/s00216-007-1768-z

[10] B. S. Hosker, "Demonstrating Principles of Spectrophotometry by Constructing a Simple, Low-Cost, Functional Spectrophotometer Utilizing the Light Sensor on a Smartphone." *Journal of Chemical Education*. 2017; 95: 178−181. DOI.10.1021/acs.jchemed.7b00548

[11] A. Scheeline, "How to design a spectrometer." Applied spectroscopy 71.10 (2017): 2237-2252.

[12] R. L. McClain, "Construction of a Photometer as an Instructional Tool for Electronics and Instrumentation." Journal of Chemical Education 91.5 (2014): 747-750. DOI: 10.1021/ed400784x

[13] W. E. Wentworth, "Dependence of the Beer-Lambert absorption law on monochromatic radiation: An experiment of spectrophotometry", *Journal of Chemical Education*, vol. 43, no. 5, p. 262, 1966. doi:10.1021/ed043p262.

[14] V. Kumar, K. D. Gill, "Photometry: Colorimeter and Spectrophotometer." In: Basic Concepts in Clinical Biochemistry: A Practical Guide. (2018) Springer, Singapore. https://doi.org/10.1007/978-981-10-8186-6_5

[15] A. Thorseth, J. Lindén, C. Dam-Hansen, "Comparison of stray light in spectrometer systems using a low cost monochromatic light source." Proceedings of CIE 2014: Lighting Quality and Energy Efficiency. International commision on illumination, 2014. pp. 557-564

[16] D. A. Skoog, F.J. Holler, S.R. Crouch, "Principles of Instrumental Analysis". 6th ed. Pacific Grove, CA: Thomson Brooks/Cole; 2006.

[17] J. R. Hamilton, J.S. White, M.B. Nakhleh. "Development of a Low-Cost Four-Color LED Photometer." *Journal of Chemical Education*. 1996; 73 (11), 1052–1054. DOI.10.1021/ed073p1052

[18] X. Liu, J. W. Locasale, "Metabolomics: A Primer," Trends in Biochemical Sciences, Volume 42, Issue 4, 2017, Pages 274-284, ISSN 0968-0004, https://doi.org/10.1016/j.tibs.2017.01.004.

[19] J. R. Idle, F.J. Gonzalez. "Metabolomics," Cell Metabolism. Vol. 6, Issue 5, 2007, p.348-351, DOI. 10.1016/j.cmet.2007.10.005.

[20] J. G. Bundy, M.P. Davey, and M.R. Viant, "Environmental metabolomics: a critical review and future perspectives," Metabolomics 5, 3 (2009). DOI. 10.1007/s11306-008-0152-0

[21] M. J. Gibney et al. "Metabolomics in human nutrition: opportunities and challenges," The American Journal of Clinical Nutrition, Volume 82, Issue 3, September 2005, Pages 497–503, https://doi.org/10.1093/ajcn/82.3.497

[22] M. Dutta, M. Joshi, S. Srivastava, I. Lodh, B. Chakravarty and K. Chaudhury, "A metabonomics approach as a means for identification of potential biomarkers for early diagnosis of endometriosis, " Mol. BioSyst., 2012, 8, 3281 DOI: 10.1039/C2MB25353D

[23] E. M. S. McNiven, J. B. German, C. M. Slupsky, "Analytical metabolomics: nutritional opportunities for personalized health," The Journal of Nutritional Biochemistry, Volume 22, Issue 11, 2011, Pages 995-1002, ISSN 0955-2863, https://doi.org/10.1016/j.jnutbio.2011.05.016.

[24] A. O'Gorman, H. Gibbons, L. Brennan, "Metabolomics in the identification of biomarkers of dietary intake," Computational and Structural Biotechnology Journal, Vol. 4, Issue 5. 2013. DOI. 10.5936/csbj.201301004.

[25] J. Sébédio, "Chapter Three - Metabolomics, Nutrition, and Potential Biomarkers of Food Quality, Intake, and Health Status," Advances in Food and Nutrition Research, Academic Press, Volume 82, 2017, Pages 83-116, ISSN 1043-4526, ISBN 9780128126332, https://doi.org/10.1016/bs.afnr.2017.01.001.

[26] M. G. Barderas *et al.*, "Metabolomic profiling for identification of novel potential biomarkers

in cardiovascular diseases," *J. Biomed. Biotechnol.*, vol. 2011, Jan. 2011, DOI. 10.1155/2011/790132.

[27] Z. Huang *et al.*, "Bladder cancer determination via two urinary metabolites: a biomarker pattern approach," *Mol. Cell. Proteomics*, vol. 10, no. 10, p. M111.007922, Oct. 2011. DOI. 10.1074.M111.007922

[28] A. Zhang, H. Sun and X. Wang, "Emerging role and recent applications of metabolomics biomarkers in obesity disease research," RSC Adv., 2017, 7, 14966 DOI: 10.1039/C6RA28715H

[29] L. Wu and X. Qu, "Cancer biomarker detection: recent achievements and challenges," Chem. Soc. Rev., 2015, 44, 2963 DOI: 10.1039/C4CS00370E

[30] E. G. Armitage, A.D. Southam, "Monitoring cancer prognosis, diagnosis and treatment efficacy using metabolomics and lipidomics," Metabolomics 12, 146 (2016). https://doi.org/10.1007/s11306-016-1093-7

[31] J. Debik, L. R. Euceda, S. Lundgren, et al. "Assessing Treatment Response and Prognosis by Serum and Tissue Metabolomics in Breast Cancer Patients," Journal of Proteome Research 2019 18 (10), 3649-3660, DOI: 10.1021/acs.jproteome.9b00316

[32] J. Griffin, J. Shockcor, "Metabolic profiles of cancer cells," Nat Rev Cancer 4, 551–561 (2004). https://doi.org/10.1038/nrc1390

[33] J. Ludwig, J. Weinstein, "Biomarkers in Cancer Staging, Prognosis and Treatment Selection," Nat Rev Cancer 5, 845–856 (2005). https://doi.org/10.1038/nrc1739

[34] K. Strimbu, J. A. Tavel "What are biomarkers?" Curr Opin HIV AIDS. 2010 Nov;5(6):463-6. doi: 10.1097/COH.0b013e32833ed177. PMID: 20978388; PMCID: PMC3078627.

[35] A. Zhang, H. Sun, P. Wang, Y. Han, and X. Wang, "Modern analytical techniques in metabolomics analysis," Analyst, 2012, 137, 293 DOI: 10.1039/C1AN15605

[36] F. Zhao, Z. Zhang, N. Ma, X. Teng, Z. Cai, M. Liu, "Untargeted metabolomics using liquid chromatography coupled with mass spectrometry for rapid discovery of metabolite biomarkers to reveal therapeutic effects of Psoralea corylifolia seeds against osteoporosis," RSC Adv., 2019, 9, 35429 DOI: 10.1039/C9RA07382E

[37] J. Grimshaw, "Electrochemical reactions and mechanisms in organic chemistry," Elsevier, 2000.

[38] R. Alcántara, et al. "Changes in oxidation state and magnetic order of iron atoms during the electrochemical reaction of lithium with NiFe2O4." Electrochemistry communications 5.1 (2003): 16-21.

[39] A. G. Tamirat, X. Guan, J. Liu, J. Luo and Y. Xia, "Redox mediators as charge agents for changing electrochemical reactions," Chem. Soc. Rev., 2020, 49, 7454 DOI:

10.1039/D0CS00489H

[40] K. J. Vetter, "Electrochemical kinetics: theoretical aspects," Elsevier, 2013.

[41] U. Guth, W. Vonau, J. Zosel, "Recent developments in electrochemical sensor application and technology—a review," 2009 Meas. Sci. Technol. 20 042002,DOI:10.1088/0957-0233/20/4/042002

[42] N. Birbilis, B. N. Padgett, R. G. Buchheit. "Limitations in microelectrochemical capillary cell testing and transformation of electrochemical transients for acquisition of microcell impedance data." Electrochimica Acta 50.16-17 (2005): 3536-3544, https://doi.org/10.1016/j.electacta.2005.01.010

[43] P. H. Gamache, D.F. Meyer, M.C. Granger, et al. "Metabolomic applications of electrochemistry/Mass spectrometry." J Am Soc Mass Spectrom 15, 1717–1726 (2004). https://doi.org/10.1016/j.jasms.2004.08.016

[44] R. Augustine, et al. "Loop-mediated isothermal amplification (LAMP): a rapid, sensitive, specific, and cost-effective point-of-care test for coronaviruses in the context of COVID-19 pandemic." Biology 9.8 (2020): 182. PMID: 32707972 PMCID: PMC7464797 DOI: 10.3390/biology9080182

[45] K. K. Ncokazi, T. J. Egan, "A colorimetric high-throughput β-hematin inhibition screening assay for use in the search for antimalarial compounds," Analytical Biochemistry, Volume 338, Issue 2, 2005, Pages 306-319, ISSN 0003-2697, https://doi.org/10.1016/j.ab.2004.11.022.

[46] H. H. Taussky, G. Kurzmann. "A microcolorimetric determination of creatine in urine by the Jaffe reaction." Journal of Biological Chemistry 208 (1954): 853-861.

[47] M. Jaffe, "Ueber den Niederschlag, welchen Pikrinsäure in normalem Harn erzeugt und über eine neue Reaction des Kreatinins," vol. 10, no. 5, pp. 391–400, Jan. 1886. DOI. 10.1515/bchm1.1886.10.5.391.

[48] J. H. Nichols, "Point of Care Testing," Clinics in Laboratory Medicine, Volume 27, Issue 4, 2007, Pages 893-908, ISSN 0272-2712, https://doi.org/10.1016/j.cll.2007.07.003.

[49] S. Yang, S. Lv, W. Zhang, Y. Cui. 2022. "Microfluidic Point-of-Care (POC) Devices in Early Diagnosis: A Review of Opportunities and Challenges" Sensors 22, no. 4: 1620. https://doi.org/10.3390/s22041620

[50] P. K. Drain, E. P. Hyle, F. Noubary, et al. "Diagnostic point-of-care tests in resource-limited settings," The Lancet Infectious Diseases, Volume 14, Issue 3, 2014, Pages 239-249, ISSN 1473-3099, https://doi.org/10.1016/S1473-3099(13)70250-0.

[51] N. Lopez-Barbosa, J. D. Gamarra, J. F. Osma, "The future point-of-care detection of disease and its data capture and handling," Anal Bioanal Chem 408, 2827–2837 (2016).

https://doi.org/10.1007/s00216-015-9249-2

[52] F. A. Castelli, G. Rosati, C. Moguet, et al. "Metabolomics for personalized medicine: the input of analytical chemistry from biomarker discovery to point-of-care tests." *Analytical and Bioanalytical Chemistry* 414, 759–789 (2022). https://doi.org/10.1007/s00216-021-03586-z

[53] V. R. Pereira, B. S. Hosker, "Low-cost (<€ 5), open-source, potential alternative to commercial spectrophotometers". *PLoS biology* (2019) 17(6), e3000321.

[54] D. Albert, M. Todt, H. Davis, "A Low-Cost Quantitative Absorption Spectrophotometer." *Journal of Chemical Education.* 2012; 89: 1432–1435. DOI.10.1021/ed200829d

[55] T. Zehetbauer, A. Plöckinger, C. Emminger, and U. D. Çakmak. "Mechanical Design and Performance Analyses of a Rubber-Based Peristaltic Micro-Dosing Pump" Actuators 10, no. 8: 198. 2021. https://doi.org/10.3390/act10080198

[56] "Elveflow Product Catalog 2023", Elveflow, https://www.elveflow.com/microfluidic-products/microfluidics-flow-control-systems/ob1-pressure-controller/ (accessed April. 01, 2023).

[57] N. A. Filatov, A. A. Evstrapov, and A. S. Bukatin. 2021. "Negative Pressure Provides Simple and Stable Droplet Generation in a Flow-Focusing Microfluidic Device" Micromachines 12, no. 6: 662. https://doi.org/10.3390/mi12060662